Benzophenone Based Cyanocinnamic acid and Carboxycoumarins as Mitochondrial Pyruvate Carrier Inhibitors for the Treatment of Nonalcoholic Steatohepatitis

A THESIS

SUBMITTED TO THE FACULTY OF THE UNIVERSITY OF MINNESOTA

BY

Jack Anthony Norman

IN PARTIAL FULFILLMENT OF THE REQUIREMENTS FOR THE DEGREE OF

MASTER OF CHEMISTRY

Dr. Venkatram Mereddy

November 2020

ACKNOWLEDGEMENTS

I would like to thank Dr. Mereddy for providing me with the knowledge and experience to become successful in the scientific field. When I first started research in his lab, I had very little experience working with some of the equipment. After numerous meetings with Dr. Mereddy's discussing my challenges, I not only became comfortable with the equipment but also with the research process. I am forever grateful for his time and scientific knowledge that he has shared during the past two years.

I would also like to thank Dr. Paul Kiprof and Dr. Steven Sternberg for being members of my committee and providing advice as I move forward with my scientific career.

I would like to thank the Department of Chemistry and Biochemistry for allowing me to be a part of the department as a researcher and teaching assistant. Through my experience as a teaching assistant, I have met numerous talented and bright students who will become leaders in the scientific field. In addition, I have gained a deeper appreciation for teachers and their level of dedication and preparation they put into their work. I am thankful for this impactful and irreplaceable experience.

I would like to acknowledge my fellow graduate and doctorate students for training me and being great friends.

Lastly, I would like to thank my grandfather, Jerry Norman, for being a voice of reason during tough times. You will be forever missed.

Abstract

Mitochondrial Pyruvate Carrier (MPC) allows pyruvate to enter the mitochondrial matrix to be used in the citric acid cycle. Inhibiting MPC has shown to be a potential treatment for Non-Alcoholic Steatohepatitis (NASH). NASH is projected to overtake Hepatitis C as the leading cause of liver transplants in the United States. The cause of NASH is elevated accumulation of lipids in hepatocytes; however, the mechanisms leading to hepatic fibrosis are unclear. Currently, there are no approved drugs for treating NASH. Recently, thiazolidiendiones have shown to be potential treatments for NASH due to their ability to inhibit MPC. However, these compounds suffer from severe side effects including osteoporosis, heart failure, and increase in bladder cancer. Cyanocinnamic acid and carboxycoumarin have been found to be highly useful pharmacophores for potent inhibition of MCT and MPC. These pharmacophores have exhibited low cytotoxicity against rapidly proliferating cancer cells. Additionally, these biologically active molecules have been found to be generally well tolerated as evidenced by our previous work in several animal models. Additionally, benzophenones are pharmacologically privileged structural entities with favorable pharmacokinetic properties. In this regard, we hypothesized that introduction of cyanocinnamic acid and carboxycoumarin onto the benzophenone scaffold would provide novel candidate compounds with favorable pharmaceutical and pharmacological properties. We also envisioned that if the synthesized compounds exhibit potent MPC inhibition, along with pharmaceutical

properties such as oral bioavailability, high metabolic stability, then they could be further developed as therapeutic agents for the treatment of NASH.

In this thesis, we have designed, synthesized, and characterized novel benzophenone containing cyanocinnamic acid and carboxycoumarin derivatives as potential MPC inhibitors. We have also synthesized a morpholino cyanocinnamic acid derivative as a water soluble MPC inhibitor. All the synthesized candidate compounds have been evaluated for their cell proliferation inhibition properties against 5 different human and murine cancer cell lines. This study indicated that the test compounds were generally not cytotoxic, even at high concentrations. The test compounds were then evaluated for their pyruvate driven respiration inhibition properties as a means to test their efficacy as potential MPC inhibitors. The benzophenone containing cyanocinnamic acid and carboxycoumarin derivatives were found to inhibit pyruvate driven respiration at 10 μM concentration.

Table of Contents

List of Figures

List of Schemes

List of Abbreviations

MPC	Mitochondrial Pyruvate Carrier
NASH	Non-alcoholic steatohepatitis
MCT	Monocarboxylate Transporter
µM	Micromollar (Molarity x 10^{-6})
NAFLD	Non-Alcoholic Fatty Liver Disease
IR	Insulin resistance
FFA	Free Fatty Acids
ROS	Reactive oxygen species
TCA	The Citric Acid
HC	High Cholesterol
OCR	Oxygen Consumption Rates
ATP	Adenosine Triphosphate
CoA	Coenzyme A
AMP	Adenosine Monophosphate
TZDs	Thiazolidinediones
mTOT	Mitochondrial Target of Thiazolidiones
PPAR	Peroxisome Proliferator-Activated Receptor
DMSO	Dimethyl Sulfoxide
^{o}C	Degrees Celsius
M	Molarity (moles/liter)
NaOH	Sodium Hydroxide
THF	Tetrahydrofuran
mM	Millimolar (Molarity x 10^{-3})

CHC	α-cyano-4-hydroxycinnamic acid
IC_{50}	inhibitory concentration where 50% of biological response is inhibited
nM	Nanomolar (Molarity x 10^{-9})
HIV	Human Immunodeficiency Virus
FDA	Food and Drug Administration
UV	Ultraviolet
Pin	Prolyl Isomerase
H_2	Molecular Hydrogen
AChE	Acetylcholinesterase
TBTU	o-(benzotriazol-1-yl)-N,N,N′,N′-tetramethyluronium tetrafluoroborate
BChE	Butyrylcholinesterase
NBS	N-bromosuccinimide
TLC	Thin Layer Chromatography
EtoAc	Ethyl Acetate
HCl	Hydrochloric Acid
$SnCl_4$	Tin (IV) Chloride
EtOH	Ethanol
$MgSO_4$	Magnesium Sulfate
NMR	Nuclear Magnetic Resonance

MTT	3-(4,5-dimethylthiazole-2-yl]-2,5-diphenyltetrazolium bromide
w/v	Weight by Volume
nm	Nanometer
rPFO	Recombinant Perfringolsyin O
PDH	Pyruvate Dehydrogenase
NADH	Nicotinamide Adenine Dinucleotide
$FADH_2$	Flavin Adenine Dinucleotide
FCCP	Carbonyl cyanide-p-trifluoromethoxyphenylhydrazone
OCR	Oxygen Consumption Rate
DCA	Dichloroacetate
PDK	Pyruvate Dehydrogenase Kinase
$ClCH_2COOH$	Chloroacetic Acid
min	Minutes
hrs	Hours
RT	Room Temperature
H_2O	Water
Cs_2CO_3	Cesium Carbonate
DMF	Dimethylformamide
$CoCl_2$	Cobalt (II) Chloride
$NaBH_4$	Sodium Borohydride
K_2CO_3	Potassium Carbonate
$POCl_3$	Phosphoryl chloride
MeCN	Acetonitrile
$AlCl_3$	Aluminum Chloride

$PhNO_2$	Nitrobenzene
BF_3	Boron Trifluoride
NH_3	Ammonia
Pd-C	Palladium on Carbon
DIEA	N,N-Diisopropylethylamine
Et_3N	Triethylamine
DCM	Dichloromethane
$SnCl_4$	Tin(IV) Tetrachloride
$MgCl_2$	Magnesium Chloride
N_2	Molecular Nitrogen
MeI	Iodomethane
$NaHCO_3$	Sodium Hypochlorite
$(PhCO)_2O_2$	Benzoyl Peroxide
CCl_4	Carbon Tetrachloride
MeOH	Methanol
^{1}H-NMR	Proton (^{1}H) Nuclear Magnetic Resonance Spectrum
^{13}C-NMR	Carbon (^{13}C) Nuclear Magnetic Resonance Spectrum
HRMS	High-Resolution Mass Spectroscopy
ESI	Electrospray Ionization
MHz	Megahertz
δ	Delta Value in ppm for NMR Spectra
J	Coupling Constant
In NMR Characterization	
s	Singlet

d	Doublet
t	Triplet
q	Quartet
m	Multiplet
dd	Doublet of Doublets
dt	Doublet of Triplets
br	Broad

Chapter 1: The Complex Biochemistry of NASH

1.A Common Features Linked to NASH

According to the American Liver Foundation, about 100 million Americans have chronic liver diseases and cirrhosis. The number of cases has been increasing concurrently with the rise in nonalcoholic fatty liver disease (NAFLD). NAFLD is an umbrella term for the spectrum of liver diseases connected by the common feature of steatosis. As the level of steatosis increases, nonalcoholic steatosis hepatitis (NASH), a more severe form of NAFLD, may develop in individuals. Although the specific mechanism leading from NAFLD to NASH is unclear, the progression has been tightly linked to insulin resistance[1, 2], abnormal mitochondrial function [3-6], oxidative damage, hepatic inflammation that promotes a state conducive to necroptosis and replacement of dead hepatocytes with a collagen matrix [7, 8]. Despite the growing number of cases and severity of NASH, there are currently no treatments to prevent or treat NASH.

To develop an effective treatment, it is critical to understand how molecular mechanisms tightly linked to NASH may contribute to the metabolic disease's existence. As previously mentioned, insulin resistance (IR) and oxidative damage have been found to be closely associated with NASH. A "two-hit hypothesis" suggested insulin resistance, the first hit, and oxidative damage, the second hit, were the initiative causes of NASH progression [25](**Figure 1**). Insulin resistance can enhance lipolysis and increases the level of serum free fatty acids (FFA). The elevation of FFA leads to delivering triglycerides from the liver to peripheral organs, which in turn induce hyper synthesis of

lipids. As a result, excessive lipid storage in the liver continues to build and an accumulation of FFA promotes the appearance of the second hit, oxidative stress [26](**Figure 1**). It is well known that β-oxidation of these FFA in mitochondria induces the formation of reactive oxygen species (ROS). Overproduction of ROS causes respiratory chain disruption and further functional defect in mitochondria, which is the main event for cytochrome c release and triggering apoptosis. Mitochondrial death is a cellular mechanism involved in the formation of hepatocellular damage, inflammation, and fibrosis in NASH pathology [27,28].

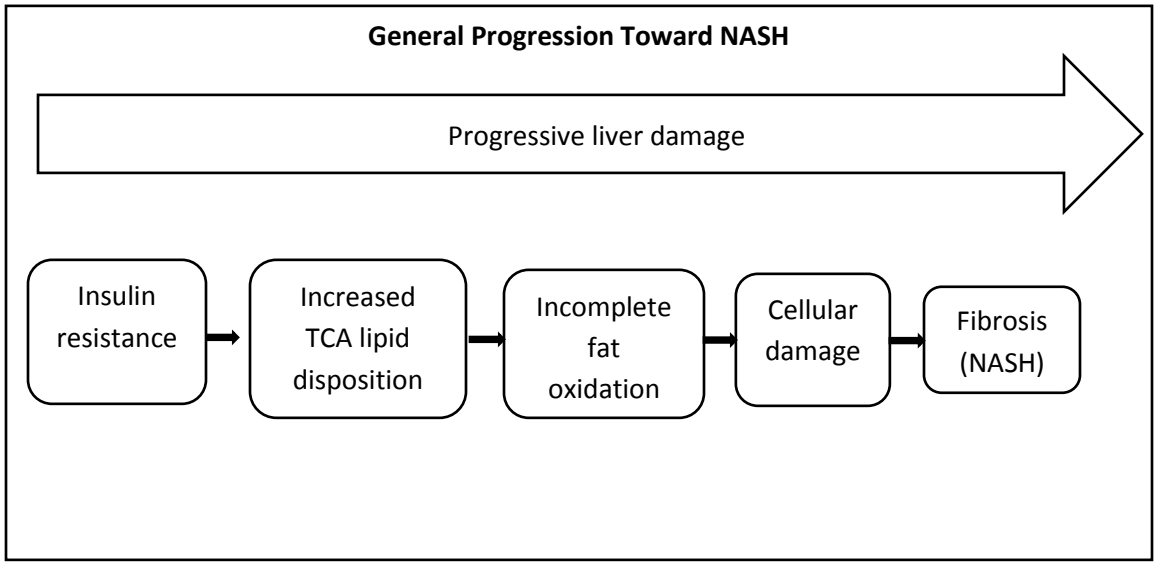

Figure 1: General progression toward NASH. Many clinical studies have documented characteristics often found in patients with NASH.

1.B Diet Contribution

Numerous clinical studies have suggested certain dietary factors, including cholesterol and fructose, are the key components in insulin resistance and oxidative

damage of the liver. Mari et al. have indicated that upon administration of a cholesterol-rich diet, free cholesterol accumulates in mitochondria causing apoptosis and lipotoxic injury to hepatocytes [29]. Normally, mitochondria are cholesterol deficient organelles compared to plasma membranes. The levels of cholesterol in mitochondrial membranes are under tight control in steroidogenic tissues or the liver, where mitochondrial cholesterol is metabolized into steroid hormones or bile acids. Diets with high cholesterol (HC), however, can impair critical mitochondrial processes. Solsona-Vilarrasa et al. conducted an experiment where mice were fed a cholesterol-enriched diet (HC) supplemented with sodium cholate to analyze the effect of cholesterol in mitochondrial function. They showed in vivo cholesterol accumulation impairs mitochondrial oxidative phosphorylation, reflected in decreased ADP-stimulated oxygen consumption rates (OCR) from complex I, which translated in decreased respiratory control [30].

Like cholesterol, fructose serves as another dietary factor that has been associated with liver toxicity. As fructose consumption rises, uric acid builds up and triggers a cascade of reactions that ultimately lead to hepatic lipogenesis and impairment of fatty acid oxidation (**Figure 2**). The specific mechanism of lipogenesis and impairment of fatty acid oxidation is complex; however, a major component of the mechanism is the reduction of aconitase-2, a Krebs cycle enzyme sensitive to oxidative stress, by uric acid. As a result, an accumulation of citrate moves into the cytoplasm and activates lipogenesis by stimulating ATP citrate lyase, a critical enzyme of de novo fatty acid synthesis [31]. The effects from uric acid are further amplified by the inhibition of enoyl CoA hydratase, an enzyme involved in fatty acid β oxidation. Hence, the accumulation of

lipids continues [32]. Jensen et al. showed that a high fructose diet induced fatty liver by both stimulating de novo lipogenesis and blocking β-fatty acid oxidation. Their evidence suggests uric acid led to increases in gut permeability and endotoxemia that exacerbates the lipogenic process in the liver, which coupled with mitochondrial dysfunction results in NAFLD [33].

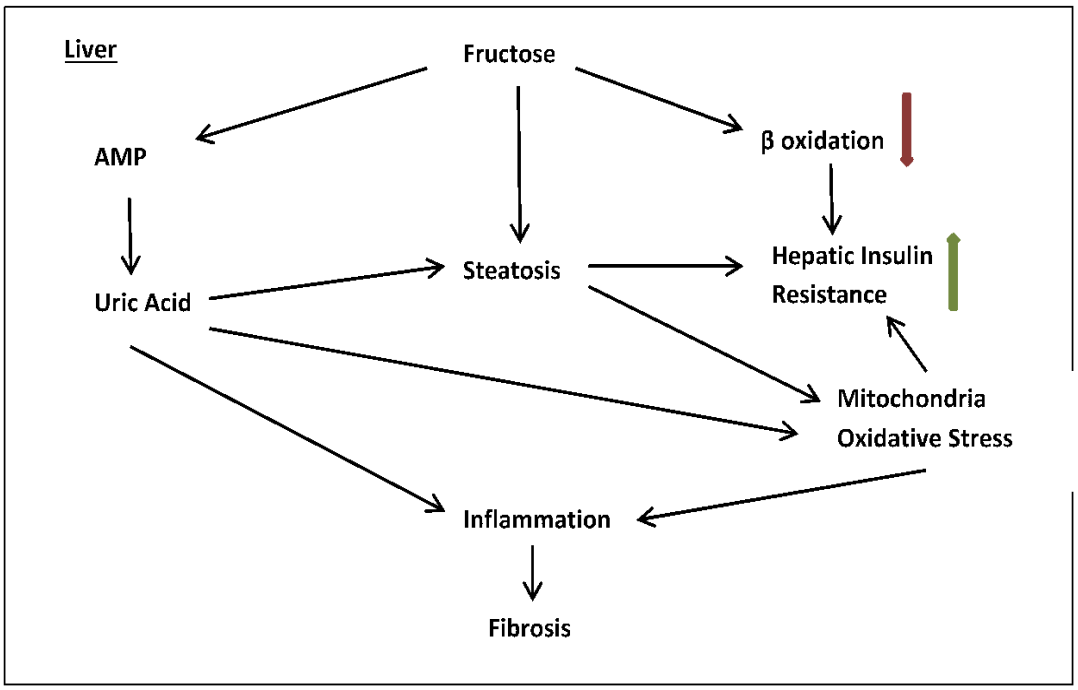

Figure 2: Fructose metabolism in liver. When fructose is ingested, lipids accumulate and hepatic insulin resistance increases. As a result, fibrosis develops and NASH occurs. Abbreviations: Adenosine monophosphate (AMP)

Just as diet can lead to NAFLD, it can also prevent it. A growing body of evidence supports the concept that a diet high in omega-3 (n-3), and low in carbohydrates such as fructose, can improve NAFLD independent of weight loss [34]. Through various mechanisms, omega-3 in fish oil have been shown to reduce lipid accumulation and liver enzyme levels, improve insulin sensitivity, and have anti-inflammatory effects [35,36, 37].

Conversely, depletion of omega-3 or increased omega-6:omega-3 (pro-inflammatory: anti-inflammatory) ratios are implicated in the development of hepatic steatosis and subsequently NAFLD/NASH [35]. While dietary changes have shown to be beneficial, the effects vary between individuals. Hence, a medication to prevent and reverse NAFLD is needed.

1.C Inhibition of MPC may Treat and Prevent NASH

Due to the ambiguous and complex progression from NAFLD to NASH, compounds with various cellular targets have been investigated. However, current research has suggested that the pathology may be regulated by the delivery of pyruvate by the mitochondrial pyruvate carrier (MPC) [9]. The MPC is a heterogeneous complex composed of two subunits, MPC1 and MPC2, found on the inner mitochondrial membrane [10]. Inhibition of either of these subunits results in a loss of pyruvate uptake and utilization [13]. Transport of pyruvate into the mitochondrial matrix is critical to numerous metabolic pathways including the citric acid (TCA) cycle. Satapati et al. have shown that over activation of the TCA cycle is part of the pathology associated with over nutrition and hepatic insulin resistance which may also contribute to NAFLD [11-12].

It is well known that the α-cyannocinnamate analog UK-5099 is a potent MPC inhibitor. Bricker et al. showed that UK-5099 interacts with MPC1, resulting in the inhibition of MPC function [15]. However, a recognition site for insulin sensitizing thiazolidinediones (TZDs) has been found in the MPC [14]. This recognition site has been named mTOT (mitochondrial target of thiazolidiones).

Initially designed for type 2 diabetes, pioglitazone and rosiglitazone served as the first generation of TZD insulin sensitizers (**Figure 3**). Recently, pioglitazone was shown to reverse hepatic fibrosis and other NASH measures in an 18-month trial [(16)]. On the other hand, Rosiglitazone, 5-fold to 10-fold more potent PPARγ agonist, improved some clinical signs tightly linked to NASH but failed to significantly affect fibrosis [(20-24)]. Despite these results, both pioglitazone and rosiglitazone bind to and activate the transcription factor PPARγ. This transcription factor improves insulin sensitivity through glucose/lipid uptake and storage in peripheral tissues, such as skeletal muscle, liver, and adipose tissue [17]. However, TZDs have undesirable and severe side effects, such as weight gain, fluid retention, and cardiovascular dysfunction [(18)]. Recently, rosiglitazone has been removed from clinical use because of its potential cardiovascular side effects [(18)].

In contrast, next-generation TZDs do not bind or activate PPARγ. Chen et al. have provided evidence of TZD analogs having similar insulin sensitizing pharmacology as produced

by pioglitazone and rosiglitazone in obese rodent models without PPARγ activation [(19)]. MSDC-0602K (**1.3**), a next-generation TZD, was found to prevent and reverse liver fibrosis and suppressed expression of stellate cell activation markers in livers of mice fed a diet rich in trans-fatty acids, fructose, and cholesterol[10]. Furthermore, mice with liver specific deletion of MPC2 were protected from development of NASH on this diet[10]. Based on these in vivo results, MSDC-0602K is in a phase 2 clinical trial to evaluate its efficacy. This investigation is a 12-month, double-blind, placebo-controlled analysis of

multiple exposures of MSDC-0602K to measure the potential of this PPARγ independent mTOT modulator to effectively treat and reverse NASH[9]. The evidence from next-generation TZDs supports further studies using MPC modulators for treating NASH.

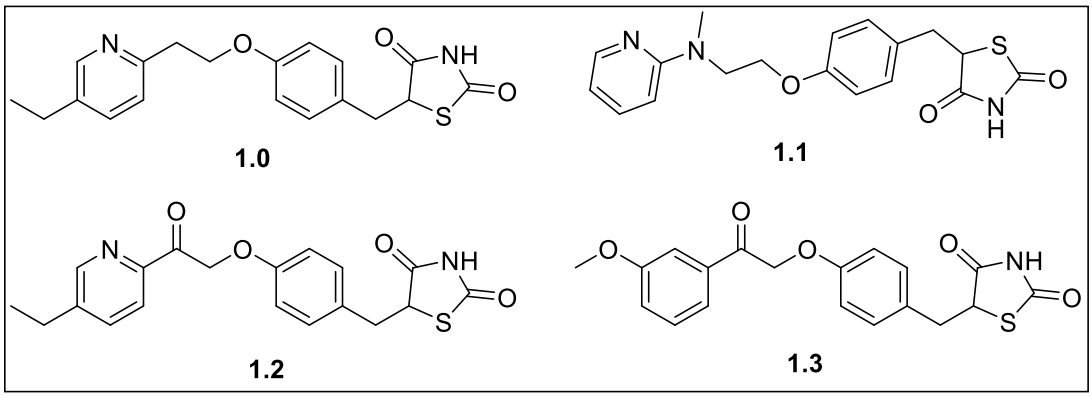

Figure 3: TZD compounds that were/are being evaluated as treatments for NAFLD.

Structures **1.0** and **1.1** represent pioglitazone and rosiglitazone respectively. They represent the first generation of TZDs due to their ability to trigger PPARγ. Structures **1.2** and **1.3** represent MSDC-0160 and MSDC-0602 respectively. They were developed by Colca et al. and are next generation TZDs because they do not activate PPARγ. MSDC-0602 is currently in phase 2 of clinical trials.

1.D Synthesis of MPC Inhibiting Small Molecule Candidates

1.D.i Thiazolidinedione (TZD) based MPC inhibitors

Darwish et al. designed TZD containing compounds as PPARγ agonists. The key TZD head group **1.5** was prepared by refluxing chloroacetic acid and thiourea **1.4** in water for 12 hours to yield pure white crystals of TZD after cooling. A Knoevenagel condensation was performed to attach the TZD group **1.5** to 4-hydroxybenzaldehyde **1.6** yielding

structure **1.7**. To increase the hydrophobicity, alkylation of **1.7** was performed with benzyl chloride **1.8** and potassium carbonate in DMSO at 80^{o}C yielding **1.9**. The resulting product was subjected to reduction with 1M NaOH, cobalt (II) chloride, and sodium borohydride in THF to produce **1.10** at 75% yield. The compound showed high PPARγ transactivation. Product **1.10** had higher intrinsic activity compared to rosiglitazone with 55-fold activation and an EC_{50} of 4.95 mM [(64)].

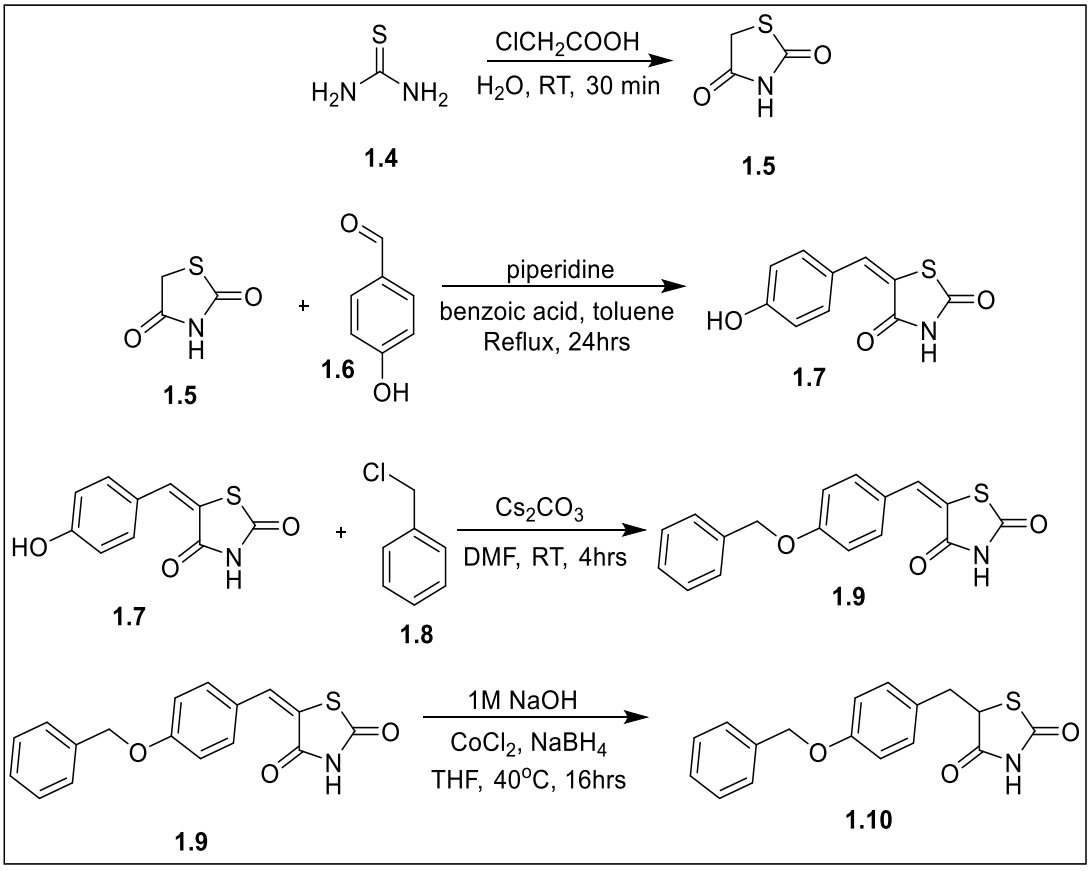

Scheme 1: Synthesis of TZD containing compound **1.10** as potential MPC inhibitor [(64)].

1.D.ii Coumarin based MPC inhibitors

Corbet et al. suggested that coumarin derivatives could serve as potent MCT1 and MPC inhibitors [38]. From this finding, previous work in Mereddy's lab involved the synthesis and biological evaluation of coumarin derivatives as potential MCT1 and MPC inhibitors [39]. To increase lipophilicity, the primary amine of **1.11** was alkylated using benzyl bromide **1.12**, potassium carbonate, and DMSO at 80°C for 12 hours. The resulting 3-(diphenylamine) phenol **1.13** was subjected to the Vilsmeier-Haack reaction at 0°C to 80°C for 4 hours. The final product **1.15** was produced at 58% yield after a Knoevenagel condensation of **1.14** with diethyl malonate followed by hydrolysis.[39] Studies are underway to determine the MPC inhibition properties of **1.15**.

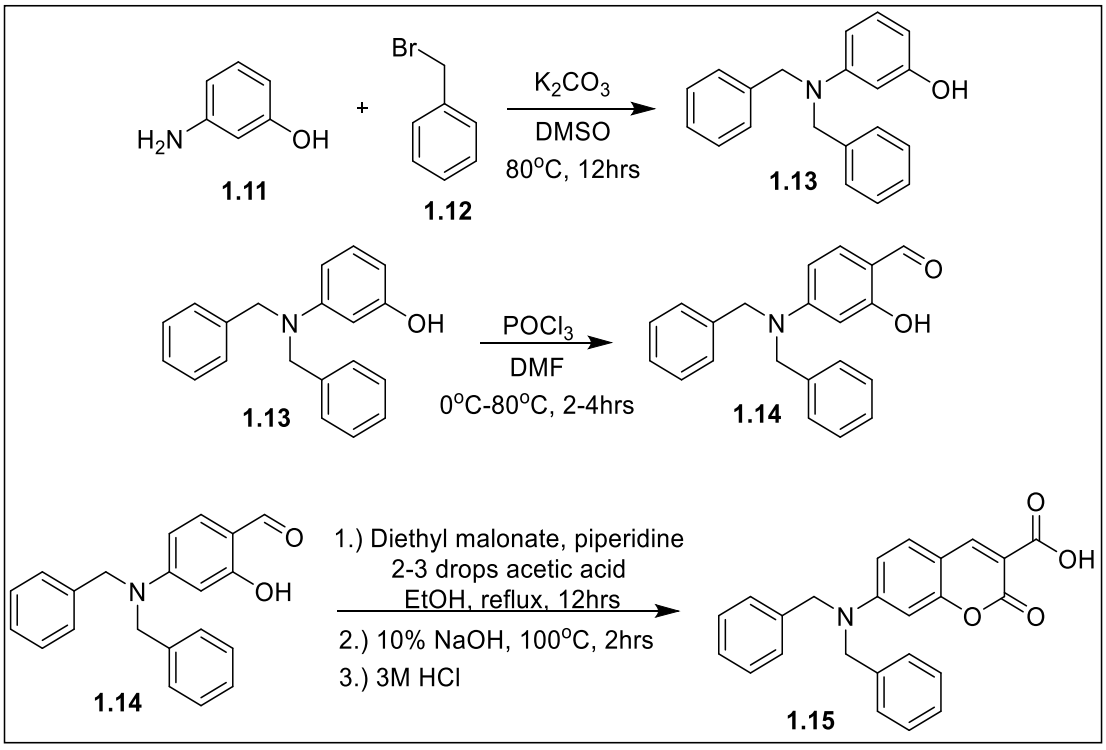

Scheme 2: Synthesis of dibenzyl coumarin derivative **1.15** as a potential MPC inhibitor [39].

1.D.iii α-cyano-4-hydroxycinnamic acids as potential MCT and MPC inhibitors.

Gurrapu et al. reported that α-cyano-4-hydroxycinnamic acid (CHC) derivatives may serve as potent MPC inhibitors. Initially investigating CHC derivatives potency against monocarboxylate transporter 1 (MCT1), they suggested that MPC may also be inhibited. This observation has been previously reported with similar cyanocinnamic acid compounds, along with aminocarboxy coumarin derivative 7ACC2 [40,38]. The lead CHC derivative **1.18** was synthesized in 76% yield via Knoevenagel condensation of **1.16** with cyanoacetic acid **1.17** using piperidine in acetonitrile (**Scheme 3**). The CHC derivative **1.18** yielded a MCT1 IC_{50} value of 8 nM [40]. Currently, studies are undergoing to determine the MPC inhibitory properties of **1.18**.

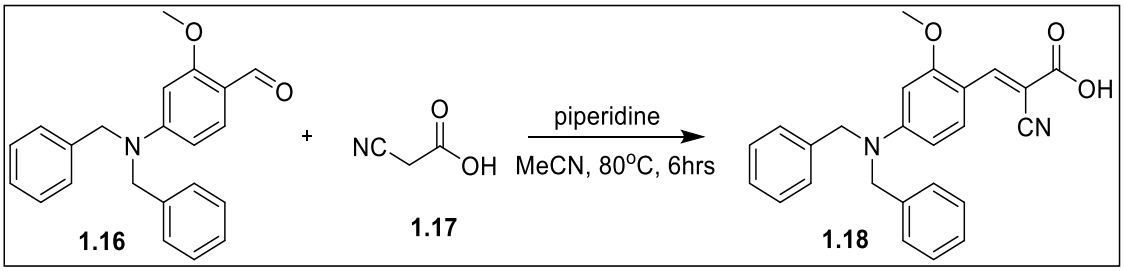

Scheme 3: Synthesis of CHC derivative **1.18** as a potential MPC inhibitor [57].

The previous work in Mereddy's lab afforded many highly potent MCT1/4 and MPC inhibitors [39, 57]. However, the synthesized derivatives were found to have low metabolic stability and rapid clearance. Due to this low metabolic stability, an additional biologically relevant benzophenone scaffold was utilized in hopes to increase biological activity and offer greater metabolic stability.

1.E Benzophenone as a structurally privileged template in medicinal chemistry.

1.E.i Benzophenone containing natural products with biological activity.

The benzophenone moiety is a biologically privileged structure that can be found in numerous natural products which exhibit biological activity such as anti-fungals, anti-HIV agents, antimicrobial agents, antiviral agents, and as antioxidants. Isolated from a *Diaporthe* sp. fungi, tenellone A has been found to exhibit antiparasitic activity of *Toxoplasma gondii* infected fibroblasts with an IC_{50} ~1.8 μM[41](**Figure 4**). Cariphenone A, a naturally occurring benzophenone found in the leaves of *Hypericum carinatum*, has been shown to exhibit antioxidant activity as evidenced by total radical-trapping antioxidant parameter assay with an IC_{50} value ~3.2 μM[42]. Isolated from a strain of *Microsphaeropsis* fungus, microsphaerin D was identified to have antibacterial properties against *Staphylococcus aureus* (MRSA) at concentrations ~1 μM[43]. Natural product malaferin A, isolated from *Malania oleifera* has been shown to ellicit anti-HIV activity *in vitro*[44](**Figure 4**).

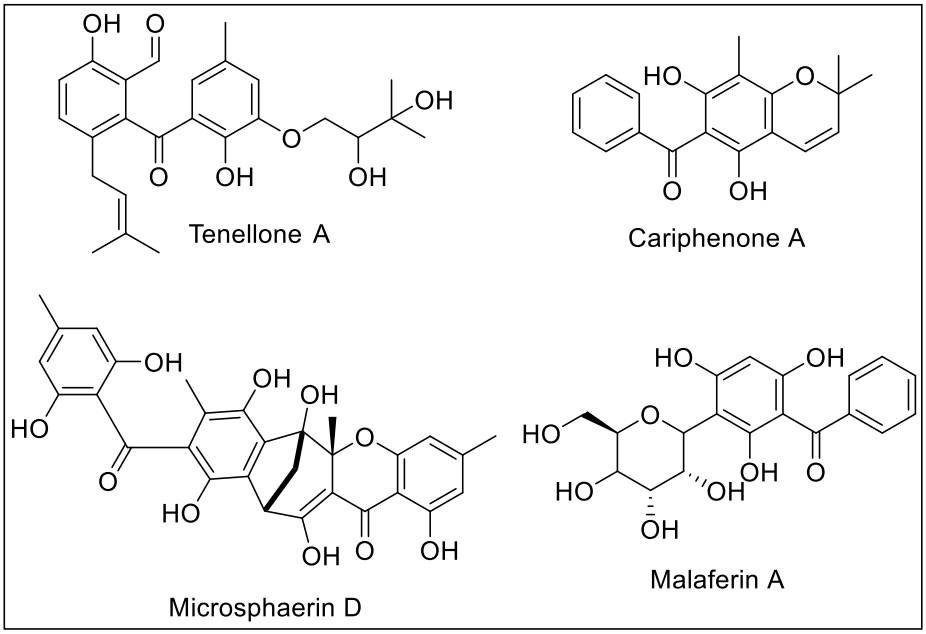

Figure 4: Benzophenone based natural products.[41-44]

1.E.ii Benzophenone structural template in FDA approved clinical agents.

While there are many biologically relevant benzophenones as natural products, there are also FDA approved drugs containing the benzophenone moiety. Used for it analgesic and antipyretic effects, ketoprofen is a commercially available non-steroidal anti-inflammatory drug[45-47](**Figure 5**). Another FDA approved drug, tolcapone, is a potent reversible catechol-O-methyltransferase inhibitor used in the treatment of Parkinson's disease[48]. For the treatment of hypercholesterolemia, benzophenone based drug fenofibrate (Tricor) is clinically used due to its peroxisome proliferator-activated receptor alpha agonist activity leading to downstream increases in lipolysis[49]. While not used directly for the treatment of a pathology, sulisobenzone and oxybenzone are commercially available sun screening agents due to their photosensitizing ability acting as UV-A/B filters[50-52](**Figure 5**).

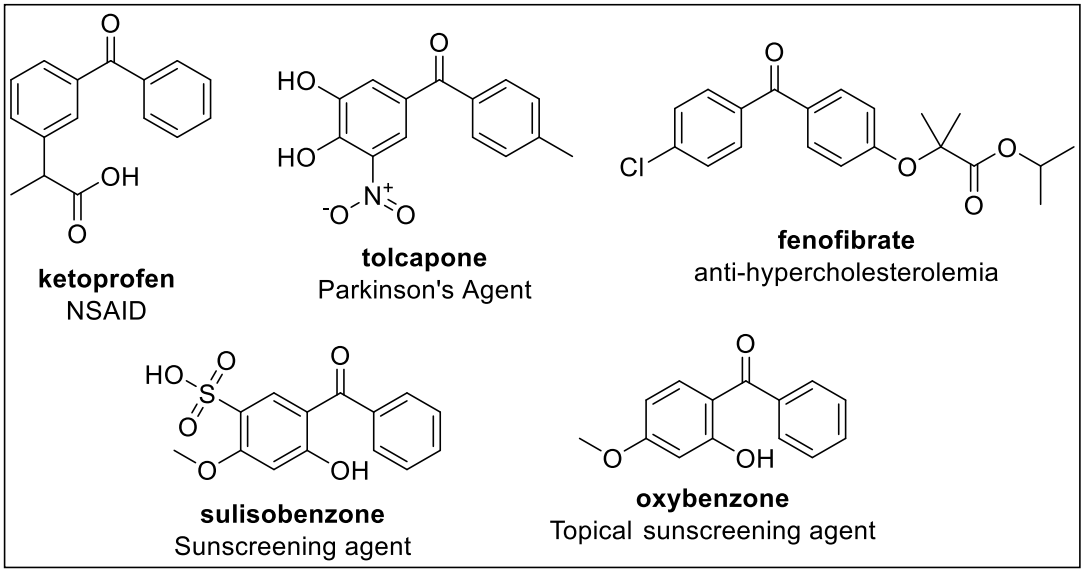

Figure 5: Clinically used benzophenone containing drugs.[45-52]

1.F Synthetic reports using benzophenone template as medicinal agents.

It is readily apparent that the benzophenone moiety is a biologically privileged structure due to its prevalence in nature and its medicinal uses in FDA approved agents. This has given rise to many research groups utilizing the benzophenone scaffold to synthesize and evaluate novel agents for the treatment of a wide variety of pathologies including: inflammation, cancer, HIV, and Alzheimer's.

1.F.i Synthetic benzophenone derivatives as anti-inflammatory agents.

Natural and synthetic benzophenones have been known for their anti-inflammatory activity. Khanum et al. synthesized 2-(2-aroyl aryloxy)-*N*-phenyl acetamide derivatives as potential anti-inflammatory agents[53](**Scheme 4**). Initially, the phenylbenzoate **1.19** was subjected to Fries rearrangement resulting in the hydroxy benzophenone **1.20**. Compound **1.20** was then alkylated with ethyl chloroacetate in SN_2 fashion resulting in ethyl (2-aroyl-4 methylphenoxy) acetates **1.21**. These products were then hydrolyzed with sodium hydroxide to obtain aroylaryloxyacetic acid **1.22**. Finally, amines **1.23** were reacted with the aroylaryloxyacetic acid resulting in 2-(2-aroyl aryloxy)-*N*-phenyl acetamide **1.24**. All the synthesized derivatives were evaluated for their anti-inflammatory activity and it was determined that chloro moiety in the meta position was essential for anti-inflammatory activity[53](**Scheme 4**).

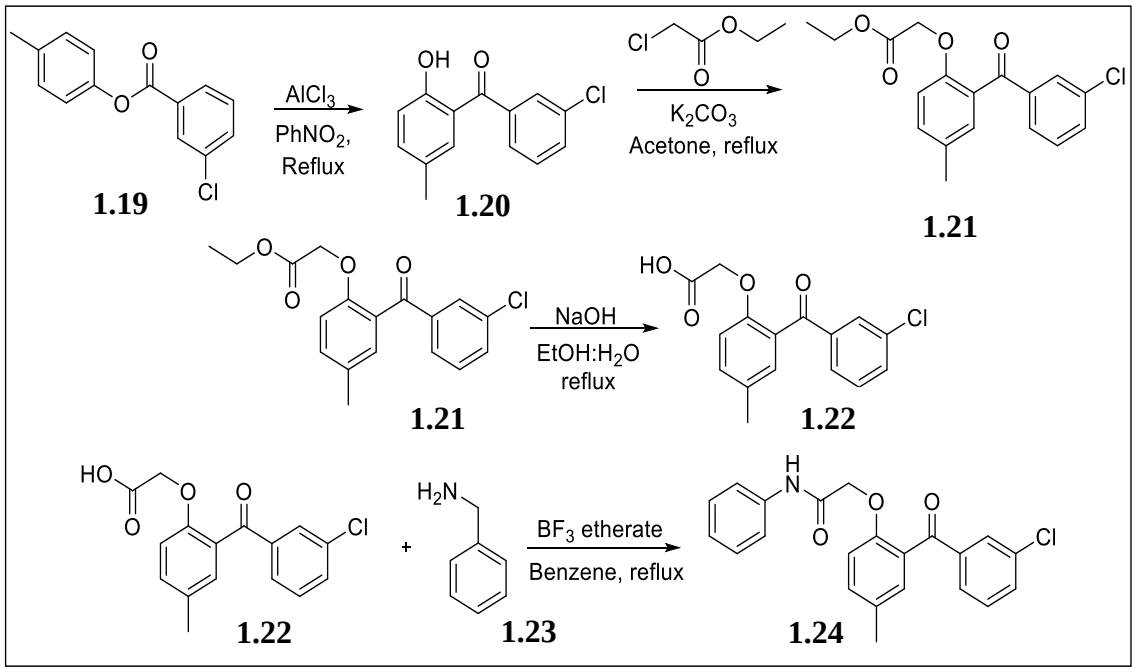

Scheme 4: Synthesis of 2-(2-aroyl aryloxy)-*N*-phenyl acetamide **1.24** as a potential anti-inflammatory agent[53].

1.F.ii Synthetic benzophenone derivatives as anticancer agents.

In 2012, Xu et al. synthesized a series of diamino derivatives of benzophenones for Pin1 inhibition (**Scheme 5**). Pin1 is a protein that is upregulated in various tumors. Synthesis began by reacting benzophenone **1.25** with ammonia under microwave irradiation resulting in aminobenzophenone **1.26**. Next the amine was reacted with ethyloxalyl monochloride resulting in amide **1.27**. This product was reduced with palladium carbon/H_2 forming the amidoaniline **1.28.** This aniline was then coupled with benzothiophene **1.29** resulting in product **1.30**. Finally, the product **1.30** was hydrolyzed with sodium hydroxide resulting in the carboxylic acid **1.31**. This final product was evaluated on the protease coupled enzyme assay showing the effects of the Pin1 activity with an IC_{50} value of ~6 μM[54](**Scheme 5**).

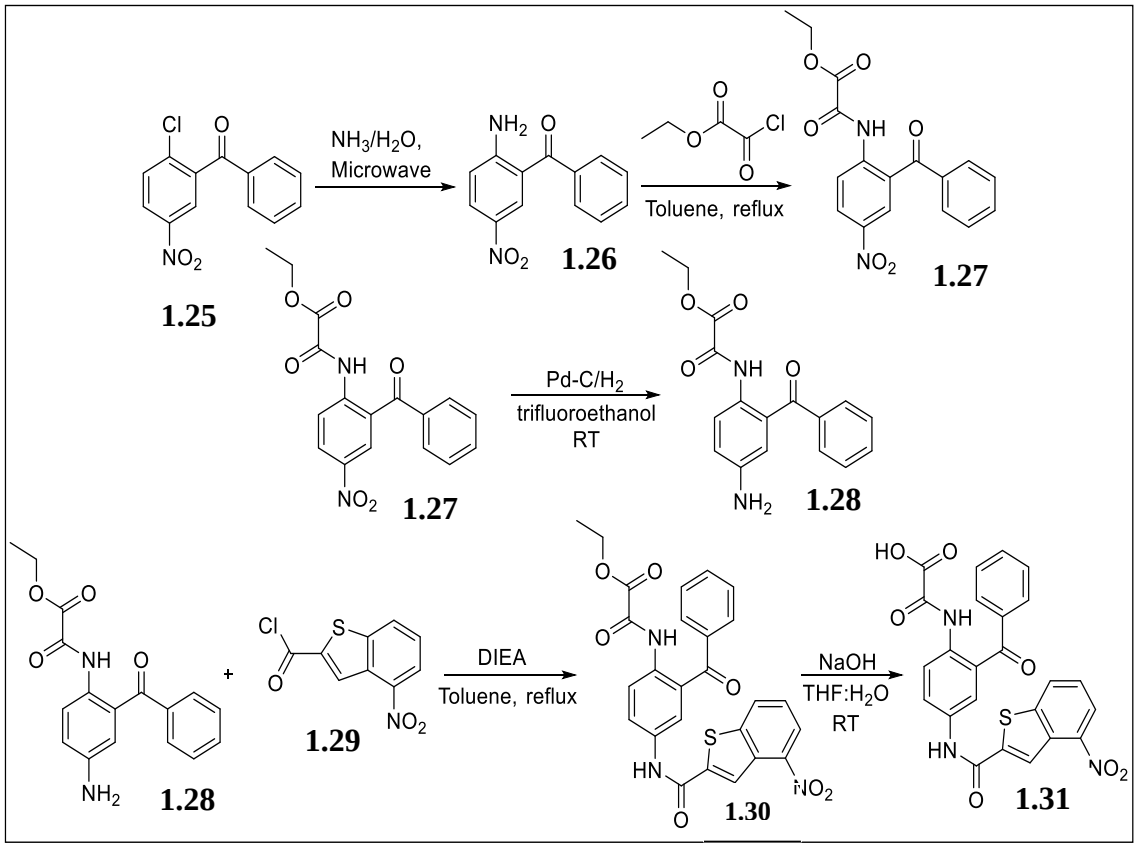

Scheme 5: Synthesis of 2-((2-benzoyl-4-(4-nitrobenzo[b]thiophene-2-carboxamido)phenyl)amino)-2-oxoacetic acid **1.31** as a potential anti-cancer agent[(54)].

Vinaya et. al. synthesized novel piperidinyl based anticancer agents for the treatment of leukemia (**Scheme 6**). The derivatives were screened for their anti-leukemia activity using human bone marrow chronic myelogenous leukemia cell line K562 and human peripheral blood acute lymphoblastic leukemia cell line CEM. The lead compounds exhibited IC_{50} values ranging from 1.6-8.0 µM in both cell lines. The synthesis involved o-alkylation of benzophenone **1.32** with chloroacetic acid in the presence of potassium carbonate as base. The newly formed carboxylic acid **1.33**

underwent amide coupling to 1,3-di(piperidin-4-yl)propane **1.34** using *o*-(benzotriazol-1-yl)-*N,N,N′,N′*-tetramethyluronium tetrafluoroborate (TBTU 10 mol%) in the presence of N-methylmorpholine to afford benzophenone piperidyl amide **1.35**. This benzophenone piperidyl amide was reacted with isocyanate or thioisocyanate in the presence of triethylamine to give final products **1.36** and **1.37** in high yields[55](**Scheme 6**).

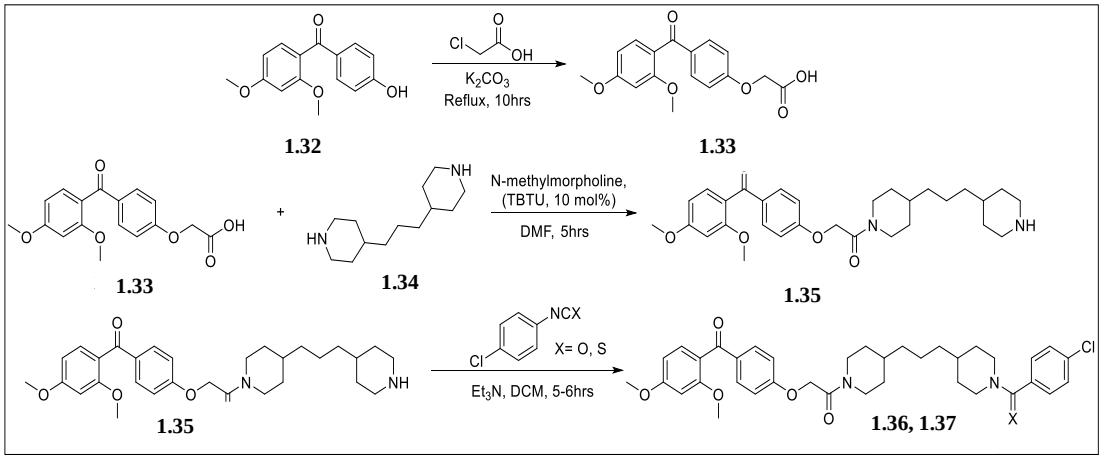

Scheme 6: Synthesis of novel benzophenone based piperdinoamides **1.36** and **1.37** as potential anti-leukemia agents[55].

1.F.iii Synthetic benzophenone derivatives as potential therapeutic agents for Alzheimer's disease.

Bettuti et. al. synthesized (4-((benzyl(alkyl)amino)methyl)phenyl)(3,4-dimethoxyphenyl)methanone based derivatives as potential acetylcholinesterase (AChE) inhibitors for the treatment of Alzheimer's disease (**Scheme 7**). The synthesized derivatives were screened for their enzymatic inhibition properties on AChE and butyrylcholinesterase (BChE) showing IC_{50} values of 0.46 and 61 µM respectively. The

synthetic pathway began by subjecting 1,2-dimethoxybenzene **1.38** to Friedel Crafts alkylation with 4-methylbenzoyl chloride **1.39** in the presence of Lewis acid $SnCl_4$ to afford **1.40**. Compound **1.40** was then subjected to Wohl-Ziegler benzylic bromination using N-bromosuccinimide (NBS) and benzoyl peroxide to give brominated product **1.41**. This bromide was further subjected to different benzyl amines **1.42** in toluene using triethylamine as base to acquire final product **1.43**[56](**Scheme 7**).

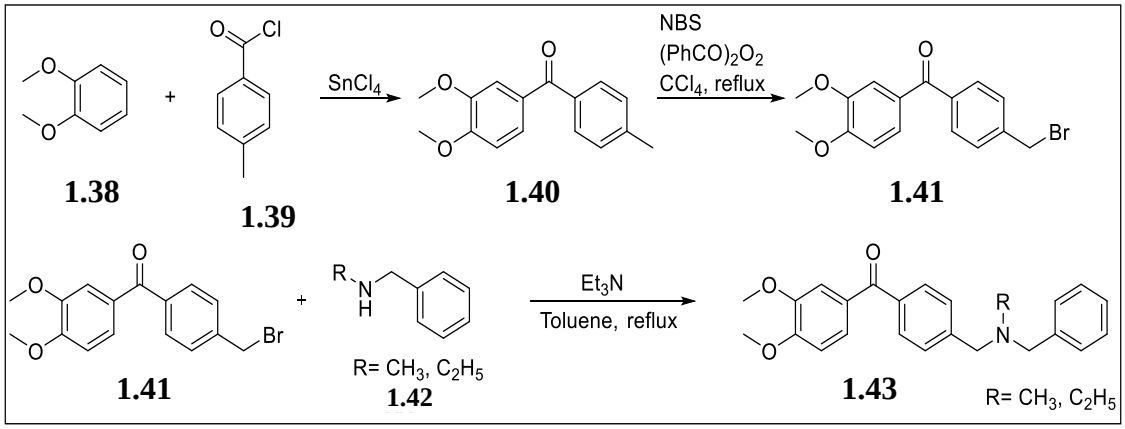

1.38 **1.39** **1.40** **1.41**

1.41 **1.42** **1.43**

Scheme 7: Synthesis of (4-((benzyl(alkyl)amino)methyl)phenyl)(3,4-dimethoxyphenyl)methanone as an potential anti-Alzheimer's agent via acetylcholinesterase inhibition[56]

Chapter 2: Results and Discussion

2.A Hypothesis and Objectives

As discussed in the introduction, cyanocinnamic acid and carboxycoumarin have been found to be highly useful pharmacophores for potent inhibition of MCT and MPC. These pharmacophores have exhibited low cytotoxicity against rapidly proliferating cancer cells. Additionally, these biologically active molecules have been found to be generally well tolerated as evidenced by our previous work in several animal models[39,57]. The compound treated animals had ~100% survival rate, normal body weight gains, and no behavioral changes. As also discussed, benzophenones are pharmacologically privileged structural entities with favorable pharmacokinetic properties[58]. In this regard, we hypothesized that introduction of cyanocinnamic acid and carboxycoumarin onto the benzophenone scaffold would provide novel candidate compounds with favorable pharmaceutical and pharmacological properties (**Figure 6**). We also envisioned that if the synthesized compounds exhibit potent MPC inhibition, along with pharmaceutical properties such as oral bioavailability, high metabolic stability, then they could be further developed as therapeutic agents for the treatment of NASH.

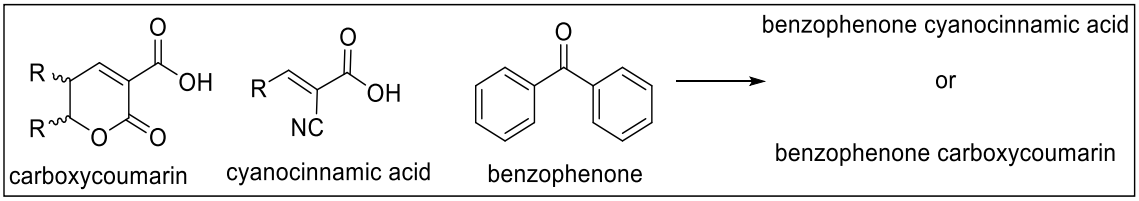

Figure 6: Benzophenone cyanocinnamic acid and benzophenone carboxycoumarin structural templates as potential MPC inhibitors.

In line with the hypothesis, the objectives of the current work include:

1.) Development of novel synthetic methodology for the creation of benzophenone containing cyanocinnamic acid and benzophenone containing carboxycoumarin.

2.) *In vitro* evaluation of the synthesized compounds as nontoxic MPC inhibitors.

2.B Synthesis of cyanocinnamic acid and carboxycoumarin benzophenone derivatives.

2.B.i Synthesis of novel benzophenone cyanocinnamic acid derivative.

Our synthetic endeavor started with commercially available 4-hydroxybenzophenone **2.1**. The phenolic hydroxy group in **2.1** was subjected to ortho formylation via Mannich reaction (**Scheme 8**)[59]. The phenol **2.1** was treated with paraformaldehyde in the presence of triethyl amine and magnesium chloride under refluxing conditions using acetonitrile as solvent. The progress of the reaction was monitored via TLC analysis. At the end of the reaction the reaction mixture was worked up with EtOAc and the resulting crude product was purified via silica gel column chromatography to obtain the ortho formylated hydroxy benzophenone **2.2**.

It was interesting to note that the formylated product **2.2** on TLC was nonpolar compared to the starting hydroxy benzophenone **2.1**. This could be due to the intramolecular hydrogen bonding between the hydroxy group and the aldehyde, forming a pseudo six membered ring. We then alkylated the hydroxy group in **2.2** to methoxy ether derivative **2.3** (**Scheme 8**). The alkylation reaction was conducted with iodomethane in the presence of potassium carbonate base using acetonitrile as solvent.

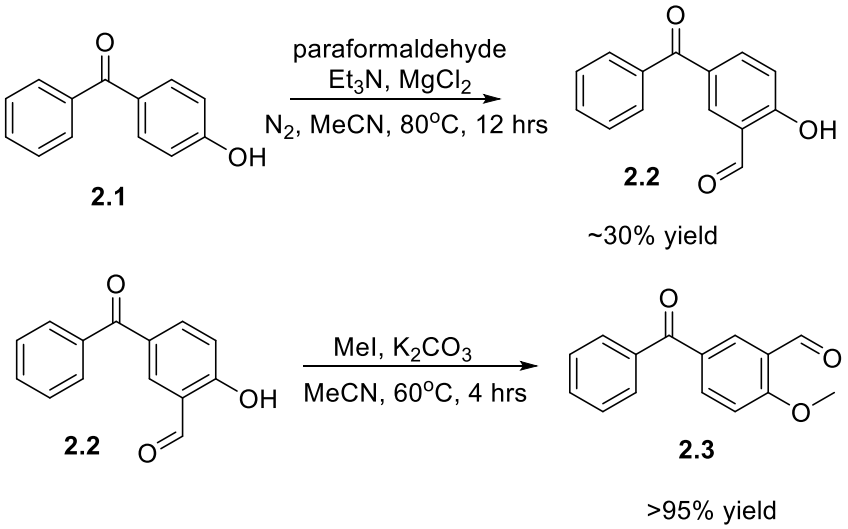

Scheme 8: Synthesis of methoxy formylbenzophenone **2.3**.

With aldehyde **2.3** in hand, we converted it into the corresponding cyanocinnamic acid via Knoevenagel condensation. The aldehyde **2.3** was treated with cyanoacetic acid using piperidine as a base in acetonitrile as solvent. After completion of the reaction, the crude reaction mixture was poured in an ice water mixture and acidified with dilute HCl.

The aqueous mixture was extracted 3 times with EtOAc to obtain the crude product **2.4**. The pure product was obtained upon repeated washing with cold diethyl ether (**Scheme 9**).

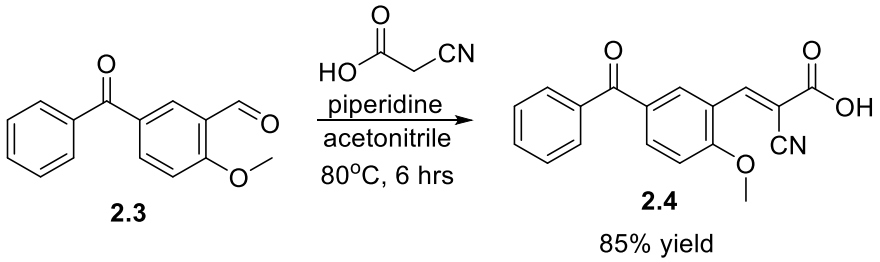

Scheme 9: Synthesis of methoxy benzophenone cyanocinnamic acid **2.4.**

2.B.ii Synthesis of novel carboxycoumarin benzophenone derivative.

We synthesized carboxycoumarin benzophenone derivative **2.7** starting from the hydroxy aldehyde **2.2** (**Scheme 10**). The Knoevenagel condensation of **2.2** with diethylmalonate **2.5** under basic conditions using piperidine gave the intermediate product **2.6**. The crude reaction mixture was then hydrolyzed with 10%NaOH in a 50:50 mixture of EtOH and water. Upon completion of the reaction, the mixture was acidified with 3M HCl to allow for the cyclization of the product. The aqueous layer was extracted 3 times with EtOAc, dried with $MgSO_4$, filtered, and concentrated using a rotary evaporator. The product **2.7** was further purified by repeated washing with diethyl ether (**Scheme 10**).

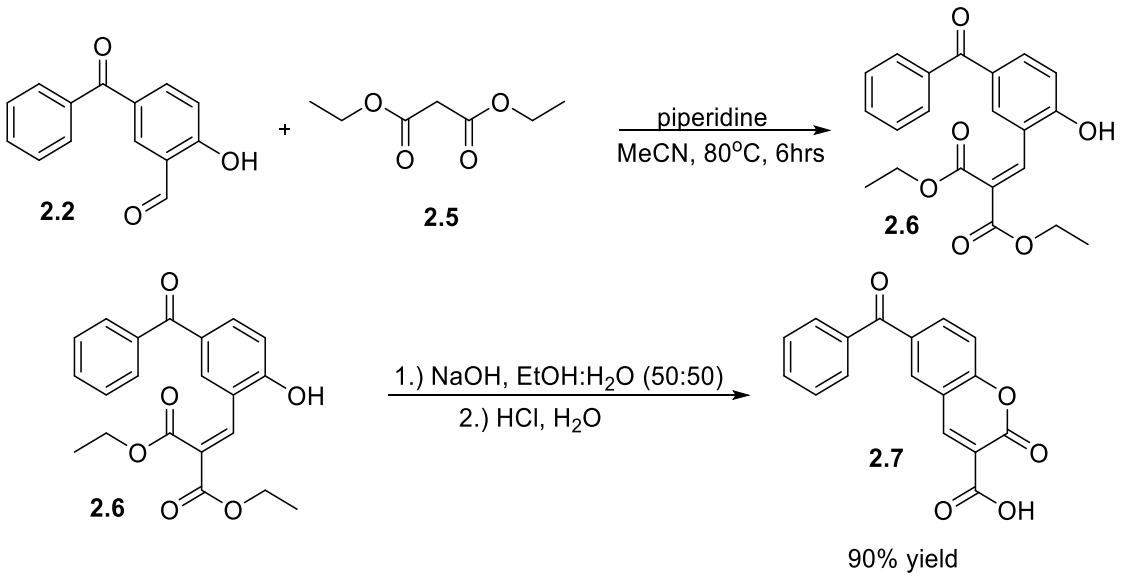

Scheme 10: Synthesis of benzophenone carboxycoumarin **2.7**.

The benzophenone cyanocinnamic acid **2.4** and carboxycoumarin **2.7** were found to be highly insoluble in water. These compounds exhibited limited solubility even in biologically compatible organic solvent DMSO. We presume that the low solubility is mainly due to the π-stacking properties flat aromatic ring. Our future work will involve the conversion of the carboxy groups in **2.4** and **2.7** to their sodium salts or solubilizing amino ester prodrugs (**Scheme 11**).

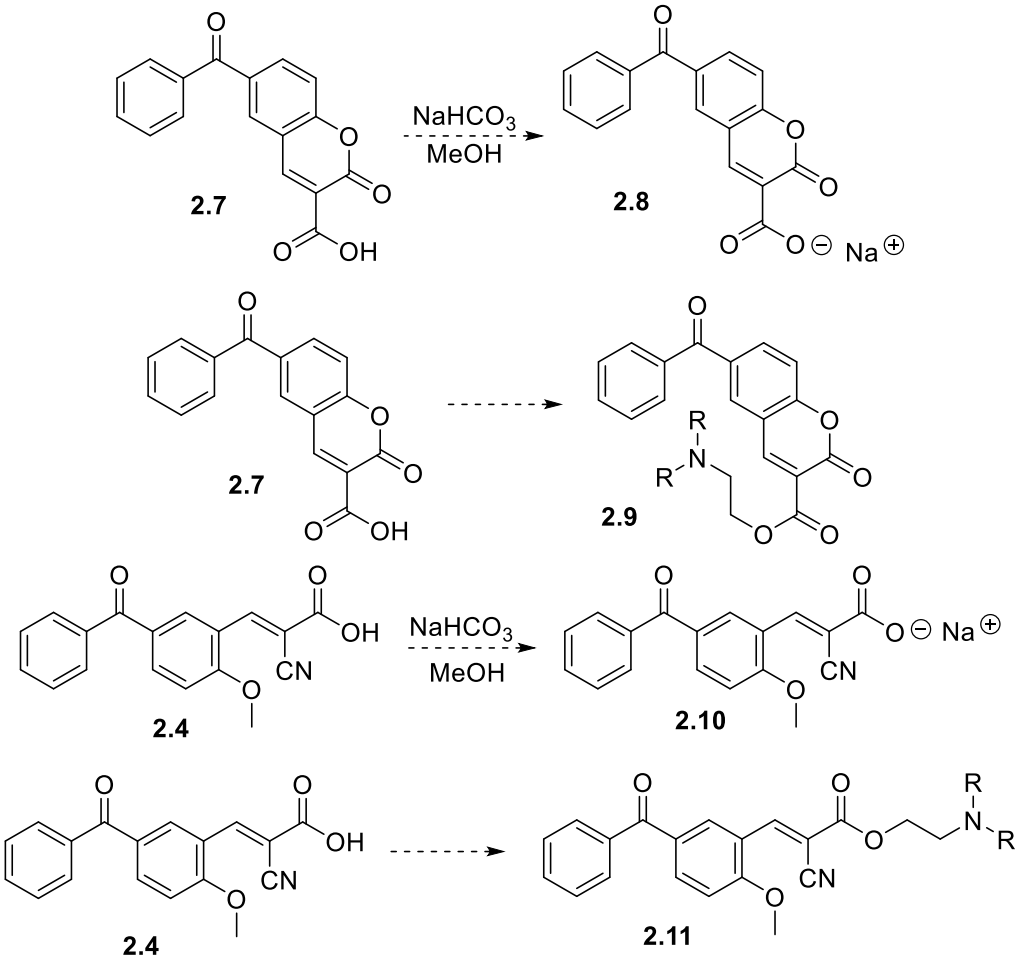

Scheme 11: Proposed future work to synthesize water soluble derivatives of cyanocinnamic acid **2.4** and carboxycoumarin **2.7** benzophenone derivatives.

2.B.iii Synthesis of novel morpholino cyanohydroxycinnamic acid (CHC).

Cyanohydroxycinnamic acid (CHC) is traditionally used as an MCT1 inhibitor and this compound also exhibits MPC inhibition properties[(60)]. CHC has been shown to

be highly nontoxic even at very high concentrations (>100mg/kg) in various mice toxicology studies. This compound has also been extensively studied as a potential therapeutic agent for the treatment of various cancers and has also been utilized as a pharmacological tool for studying metabolism based biochemical reactions[60]. However, CHC is a low molecular weight compound (189 g/mol) with poor pharmacokinetic and pharmacodynamic properties. Moreover, CHC requires high concentrations to elicit MCT and MPC inhibition properties due to its lack of potency. The poor pharmacological and pharmaceutical properties of CHC make it undesirable to be further developed as a clinical agent. In this regard, we envisioned to synthesize morpholino CHC **2.15** as a water soluble CHC derivative with improved drug like properties. Morpholine **2.13** is a structurally privileged moiety, this unit is found in many clinically used drugs for a plethora of diseases[61]. It has been extensively studied that introduction of morpholine to a lead candidate compound often improves the water solubility, oral bioavailability, and other desirable drug-like properties. In this regard, the non-benzophenone cyanocinnamic acid derivative **2.15** was designed to study the pharmacological and pharmaceutical properties and compare its efficacy as an MPC inhibitor against the benzophenone derivatives **2.4** and **2.7**.

The synthesis of **2.15** was achieved in a 2-step protocol (**Scheme 11**). The first step involved the Mannich reaction of commercially available 4-hydroxybenzaldehyde **2.12** with morpholine **2.13** and paraformaldehyde. At the end of the reaction, EtOH was removed using a rotary evaporator and the crude product was extracted with water and EtOAc. The organic layer was separated, dried with $MgSO_4$, filtered, and concentrated

using rotary evaporator. The pure product was obtained after purification using silica gel column chromatography in 65% yield. The aldehyde **2.14** was subjected to Knoevenagel condensation with cyanoacetic acid under standard basic conditions. The reaction mixture was poured over dilute HCl in ice water and was extracted with EtOAc to obtain the crude product **2.15**. The pure product was obtained upon repeated washings with diethyl ether at 95% yield (**Scheme 11**).

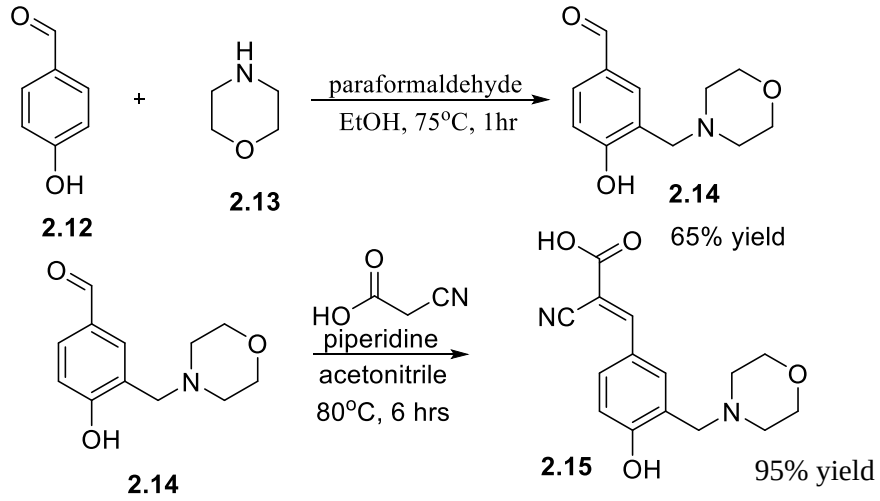

Scheme 12: Synthesis of morpholino cyanocinnamic acid **2.15**.

All the intermediates and the final candidate compounds were thoroughly characterized by ^{1}H and ^{13}C NMR, and mass spectrometry analysis.

2.C *In vitro* biological evaluation of candidate compounds 2.4, 2.7, and 2.15.

2.C.i Cell proliferation inhibition studies of candidate compounds 2.4, 2.7, and 2.15.

Our goal was to develop therapeutic agents for the treatment of NASH, the candidate compounds should be nontoxic at high concentrations. One way to quickly evaluate their toxicity is to test their cell inhibition properties on rapidly proliferating cancer cells. In this regard, we have chosen a wide panel of human and murine cancer cell lines with varying proliferation rates. The cell lines included human triple negative breast cancer (MDA-MBA-231), human pancreatic cancer cell line (MIAPaCa-2), human colorectal adenocarcinoma (WiDr), human breast cancer (MCF-7), murine breast cancer (67NR), and murine metastatic breast cancer cell line (4T1) cell line.

Cell proliferation inhibition studies were carried out using a standard 3-(4,5-dimethylthiazole-2-yl]-2,5-diphenyltetrazolium bromide (MTT) cell viability assay. In this assay MTT is converted to insoluble formazan via mitochondrial reductase after incubation of the cancer cells with MTT for 4 hours. The insoluble formazan can be solubilized using 10% w/v sodium dodecyl sulfate and absorbance at 570 nm can then be taken. Untreated wells will have the highest absorbance reading and will serve as a reference for uninhibited cell proliferation. Comparing the compound treated absorbances to the uninhibited references allows for percent survival values to be calculated. The percent cell survival can be plotted against the log of concentration to generate a dose response curve. The concentration where 50% of cell proliferation inhibition is inhibited is known as the IC_{50} value. This value serves as a representative value of how potent the test compounds are in inhibiting cell growth, the lower the concentration means the higher the compounds potency at inhibiting cell proliferation.

After screening candidate compounds **2.4**, **2.7**, and **2.15** against our panel of cancer cell lines it was found that all derivatives are highly nontoxic at concentrations up to 100 µM. Encouraged by this result, we further carried studies to determine the metabolic inhibition properties of the candidate compounds using Seahorse XFe96 Analyzer pyruvate driven respiration assay.

2.C.ii Pyruvate driven respiration assay of candidate compounds.

Literature reports indicate that synthesized compounds based on cyanoacrylic acid and coumarin carboxylic acid templates inhibit the mitochondrial pyruvate carrier (MPC) in vitro[(62-63)]. In this regard, we envisioned that compounds **2.7** and **2.4** would similarly inhibit the MPC due to the presence of the respective pharmacophores. To investigate this, we established a Seahorse XFe96 based assay wherein permeabilized cells can be offered pyruvate, and respective oxygen consumption rates can be directly associated with pyruvate oxidation. Hence, this assay offers a means to test the capacity of candidate compounds on inhibiting pyruvate driven respiration, and potentially, the MPC. In this assay, metastatic breast cancer cell line 4T1 was utilized as we have previously identified this cell line as highly oxygen consuming in nature with large levels of mitochondrial respiration when compared to other metabolic pathways. Further, we have previously characterized that MPC is expressed at readily detectable levels, suitable for functional MPC based assays. Briefly, 4T1 cells were seeded in Seahorse XFe96 well plates and incubated overnight. Cells were then washed with MAS buffer free of metabolic substrates and were equilibrated for 1 hour. Cells were then first offered test compounds **2.7** or **2.4** at 10 µM followed by permeabilization with recombinant perfringolsyin O

(rPFO, 1nM, **Figure 7**). To permeabilized cells pyruvate was added, in combination with downstream TCA cycle intermediate malate, PDK inhibitor dichloroacetate, and proton uncoupler FCCP to stimulate maximal pyruvate driven respiration (**Figure 7**). Respiratory processes were then completely blocked with subsequent injection of complex I and III inhibitor cocktail rotenone and antimycin A, respectively (**Figure 7**). These results indicated that both candidate compounds **2.7** and **2.4** potently inhibited pyruvate driven respiration in permeabilized 4T1 cells, consistent with MPC inhibition (**Figure 7**). To further characterize these candidate compounds as specific MPC inhibitors, our future studies will involve investigating the capacity of compounds **2.7** and **2.4** to inhibit respiratory processes linked with other metabolic substrates, namely complex I mediated glutamate (NADH driven), and complex II mediated succinate ($FADH_2$ driven) respiratory processes. If candidate compounds are specific MPC inhibitors, these respiratory processes should be unaffected by compound treatment, bolstering the results presented in **Figure 7** as MPC mediated inhibition. Further, reversibility of the inhibitory characteristics of compound **2.7** or **2.4** with membrane permeable methyl pyruvate will further illustrate specific MPC targeting, and will disqualify other pyruvate processing enzymes (i.e. pyruvate dehydrogenase) as the target of our compounds.

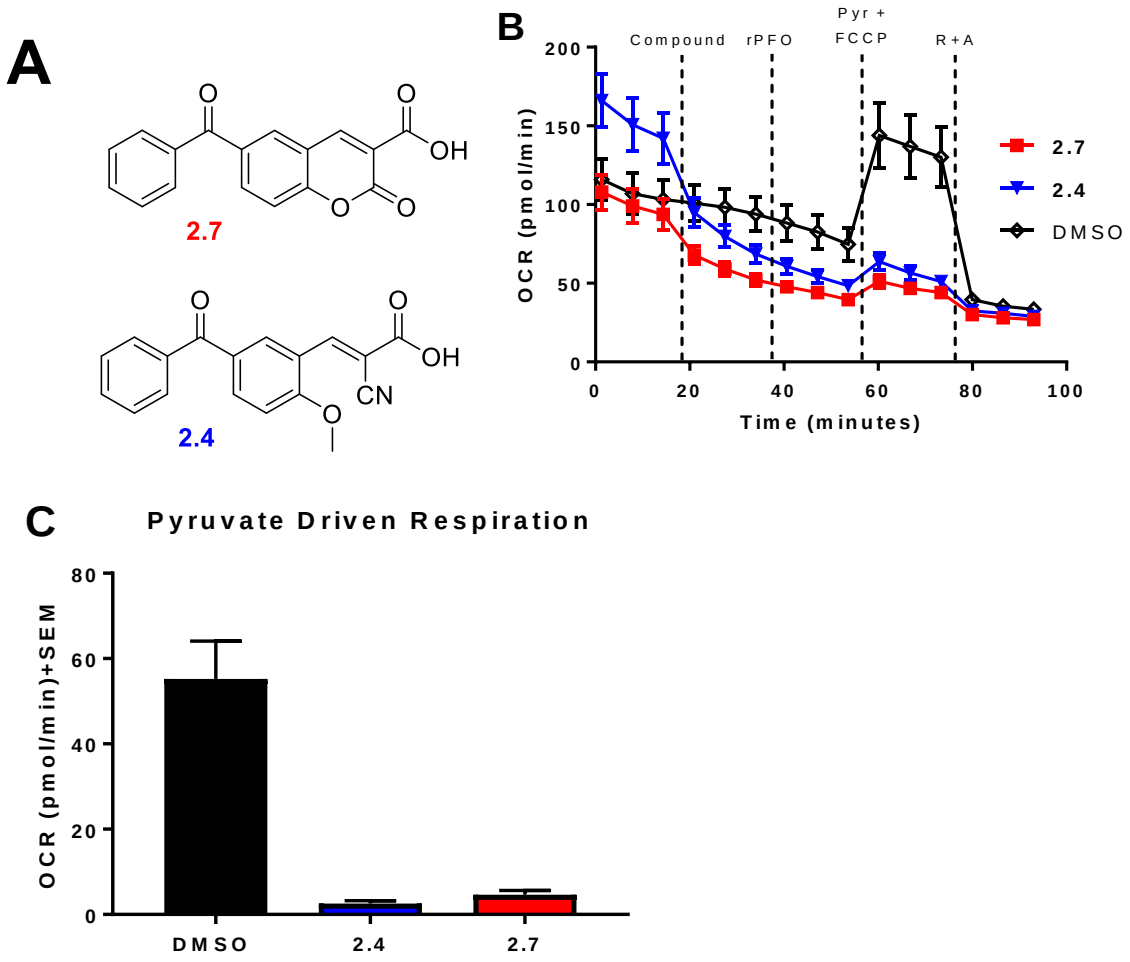

Figure 7. (**A**) Lead candidate compounds **2.7** and **2.4** potently and acutely inhibit pyruvate driven respiration in permeabilized 4T1 cells. (**B**) Real time metabolic profile of the oxygen consumption rate (OCR, pmol/min) exhibited by 4T1 cells following successive injection of test compound (**2.7** or **2.4**), rPFO, pyruvate cocktail (pyruvate, malate, dichloroacetate (DCA) and FCCP), and rotenone + antimycin A (R+A). (**C**) Pyruvate driven maximal respiration is inhibited by compound **2.7** and **2.4**. Bar graph represents the change in OCR before and after injection of pyruvate cocktail under differing treatment conditions.

2.E Conclusion and future directions

In conclusion, we have designed, synthesized, and characterized novel benzophenone containing cyanocinnamic acid and carboxycoumarin derivatives as potential MPC inhibitors. We have also synthesized a morpholino cyanocinnamic acid derivative as a water soluble MPC inhibitor. All the synthesized candidate compounds have been evaluated for their cell proliferation inhibition properties against 5 different human and murine cancer cell lines. This study indicated that the test compounds were generally not cytotoxic, even at high concentrations. The test compounds were then evaluated for their pyruvate driven respiration inhibition properties as a means to test their efficacy as potential MPC inhibitors. The benzophenone containing cyanocinnamic acid and carboxycoumarin derivatives were found to inhibit pyruvate driven respiration at 10 μM concentration.

Based on this encouraging preliminary data, our future studies will include detailed mechanistic studies to calculate the IC_{50} values for MPC inhibition, in vivo systemic toxicity studies in mice, in vivo studies in mice as potential agents for the treatment of NASH.

Chapter 3: Experimental Synthesis and Biological Assays.

3.A Synthetic procedures.

Synthesis of 4-hydroxy-3-(morpholinomethyl) benzaldehyde via Mannich reaction

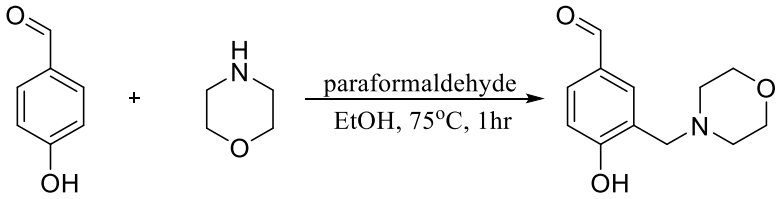

Morpholine (1 mmol) and paraformaldehyde (2.5 mmol) were stirred in EtOH (15 mL) at 75 ^{o}C for 30 minutes to allow iminium ion formation. To the reaction mixture, 4-hydroxybenzaldehyde (1.5 mmol) was added and the reaction was refluxed at 75 ^{o}C for 1 hour. Reaction progress was monitored via TLC (40% EtOAc/hexanes) for the consumption of 4-hydroxybenzaldehyde. Upon completion of the reaction, the solvent was removed using a rotary evaporator. Crude product was purified using silica gel column chromatography (40% EtOAc/hexanes) to give pure 4-hydroxy-3-(morpholinomethyl) benzaldehyde in 65% yield.

General procedure for the alkylation of 4-hydroxy-3-(morpholinomethyl) benzaldehyde under Knovenagel condensation conditions

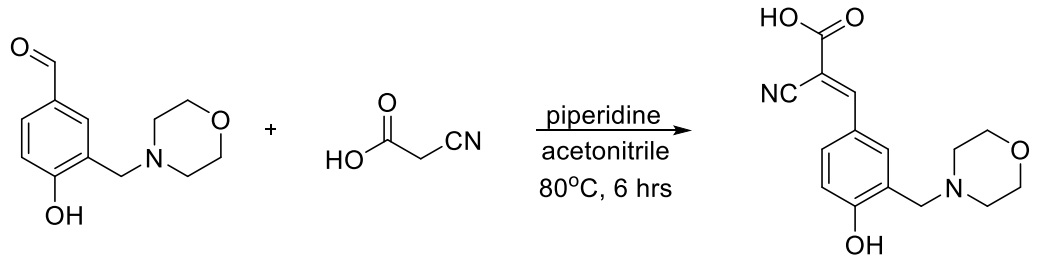

To a solution containing piperidine and 4-hydroxy-3-(morpholinomethyl) benzaldehyde (1.0 mmol) dissolved in acetonitrile (15 mL), an activated methylene (2.1 mmol) was added to the reaction and refluxed at 80^{o}C for 6 hours. The reaction progress was monitored by TLC (50% EtOAc/hexanes) to monitor the alkylation of 4-hydroxy-3-(morpholinomethyl) benzaldehyde. Upon consumption of the starting aldehyde, the reaction was quenched by pouring into dilute HCl at 0°C and extracted with EtOAc (3x75 mL). The organic layer was then dried over anhydrous $MgSO_4$ and concentrated using a rotary evaporator to yield the alkylated product.

Synthesis of 5-benzoyl-2-hydroxybenzaldehyde

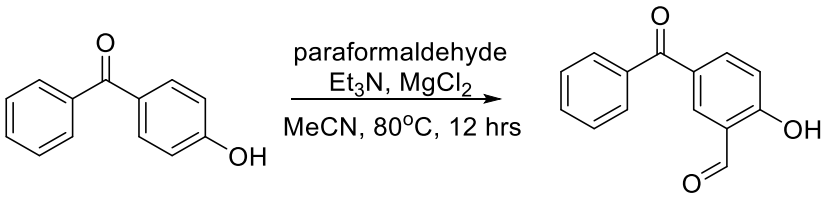

A solution containing 4-hydroxybenzophenone (1.0 mmol), $MgCl_2$ (3.5 mmol), triethylamine (2.5 mmol), and paraformaldehyde (3.5 mmol) dissolved in anhydrous acetonitrile (25 mL) was refluxed at 80^{o}C for 12 hours under nitrogen. The reaction progress was monitored by TLC (10% EtOAc/hexanes) for the formylation of 4-hydroxybenzophenone. Upon completion of the formylation, the reaction was quenched by pouring into dilute HCl at 25°C and extracted with EtOAc (3x75 mL). The organic layer was then dried over anhydrous $MgSO_4$ and concentrated using a rotary evaporator. The crude product was purified using silica gel column chromatography (8% EtOAc/hexanes) to give pure 5-benzoyl-2-hydroxybenzaldehyde in 30% yield.

Synthesis of diethyl 2-(5-benzoyl-2-hydroxybenzylidene)malonate under Knovenagel condensation conditions

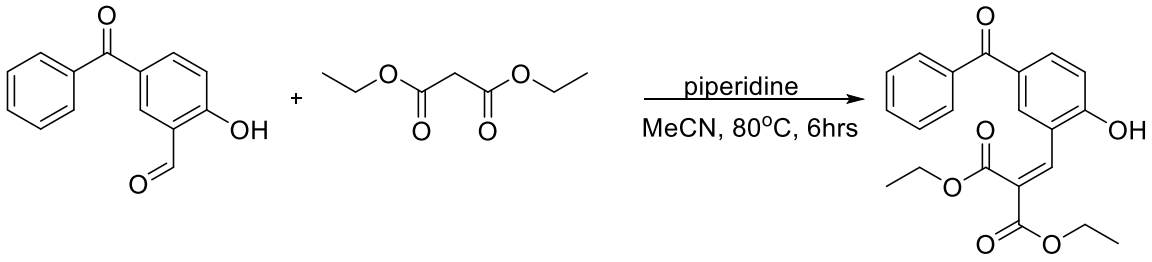

To a solution containing 5-benzoyl-2-hydroxybenzaldehyde (1.0 mmol) and piperdine (1.8 mmol) dissolved in acetonitrile (15 mL), diethylmalonate (2.2 mmol) was added to the reaction and refluxed at 80^{o}C for 6 hours. Reaction progress was monitored via TLC (40% EtOAc/hexanes) for the consumption of 5-benzoyl-2-hydroxybenzaldehyde. Upon completion of the reaction, acetonitrile was removed using a rotary evaporator. Following evaporation of solvent, product was extracted (EtOAc 3x20mL), dried with $MgSO_4$ filtered and solvent was removed using rotary evaporator to obtain crude 2-(5-benzoyl-2-hydroxybenzylidene)malonate.

Synthesis of 6-benzoyl-2-oxo-2H-chromene-3-carboxylic acid via sodium hydroxide hydrolysis

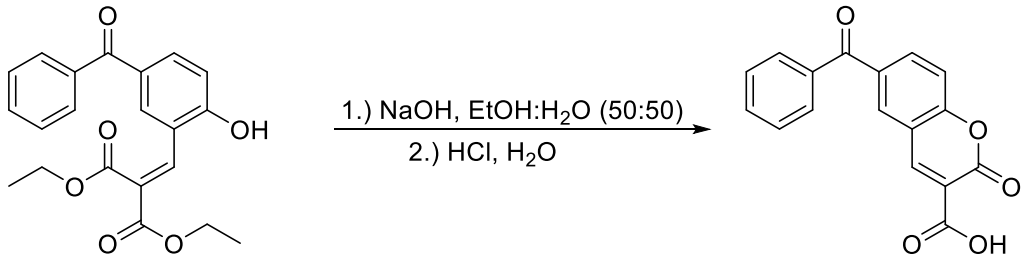

The crude 2-(5-benzoyl-2-hydroxybenzylidene)malonate was refluxed in 50% EtOH:H_2O containing 10% NaOH for 12 hrs. Reaction progress was monitored via TLC (50% EtOAc/hexanes). Once complete, the reaction was poured over 10% HCl and extracted with EtOAc (3x75 mL). The organic layer was then dried over anhydrous $MgSO_4$ and concentrated using a rotary evaporator giving the final product 6-benzoyl-2-oxo-2H-chromene-3-carboxylic acid in 90% yield.

Synthesis of 5-benzoyl-2-methoxybenzaldehyde

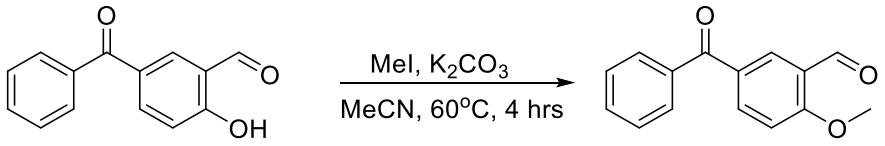

To a solution containing 5-benzoyl-2-hydroxybenzaldehyde (1.0 mmol) and potassium carbonate (2.5 mmol) dissolved in acetonitrile (15 mL), iodomethane (1.8 mmol) was added and refluxed at 60^{o}C for 4 hours. Reaction progress was monitored via TLC (25% EtOAc/hexanes) for the consumption of 5-benzoyl-2-hydroxybenzaldehyde. Once complete, the reaction was poured into water and extracted with EtOAc (3x75 mL). The organic layer was then dried over anhydrous $MgSO_4$ and concentrated using a rotary evaporator giving the final product 5-benzoyl-2-methoxybenzaldehyde in 96% yield.

Synthesis of (E) -3-(5-benzoyl-2-methoxyphenyl)-2-cyanoacetic acid under Knovenagel condensation conditions

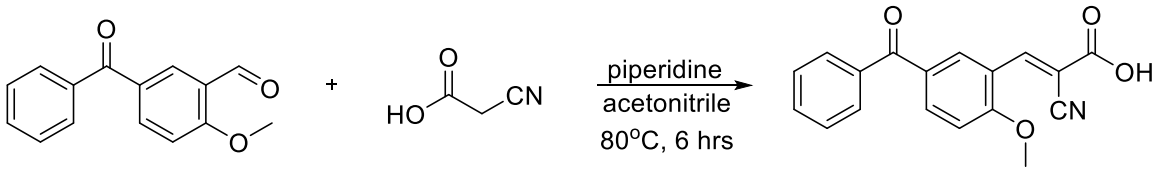

To a solution containing 5-benzoyl-2-methoxybenzaldehyde (1.0 mmol) and piperidine (1.8 mmol) dissolved in acetonitrile (15 mL), cyanoacetic acid (2.2 mmol) was added to the reaction and refluxed at 80^{o}C for 6 hours. The reaction progress was monitored by TLC (80% EtOAc/hexanes) to monitor the alkylation of 5-benzoyl-2-methoxybenzaldehyde. Upon completion of the alkylation, the reaction was quenched by pouring into dilute HCl at 0°C and extracted with EtOAc (3x75 mL). The organic layer was then dried over anhydrous $MgSO_4$ and concentrated using a rotary evaporator to yield (E) -3-(5-benzoyl-2-methoxyphenyl)-2-cyanoacetic acid at 85% yield.

3.B *In vitro* experimental procedures.

Cell Culture

MDA-MB-231 cells (ATCC) were grown in DMEM supplemented with 10% FBS and penicillin-streptomycin (50 µg/ml). MIA PaCa-2 cells (ATCC) were cultured in DMEM supplemented with 10% FBS, 2.5% horse serum and penicillin-streptomycin (50 µg/ml). 4T1 cells (ATCC) and 67NR (ATCC) were cultured in RPMI-1640 supplemented with 10% FBS and penicillin-streptomycin (50 µg/ml). MCF7 cells (Masonic Cancer Center) were grown in α-MEM supplemented with 6% FBS, penicillin-streptomycin (50µg/ml), epidermal growth factor (0.0125 g/mL), hydrocortisone (0.001 mg/mL), 1X NEAA, insulin (0.001 mg/mL), HEPES (12 mM), sodium pyruvate (0.5 mM). WiDr cells (ATCC) were grown in MEM supplemented with 10% FBS and penicillin-streptomycin (50 µg/ml). All cells were incubated at 37^{o}C and 5% CO_2.

MTT Cell Proliferation Assay

Confluent cell cultures were treated with trypsin and resuspended at $5x10^4$ cells/mL. To a 96-well plate, 100 µl of the $5x10^4$cells/mL solution were added and allowed to incubate at 37^{o}C, 5% CO_2 for 24 hours. Compounds were then added and allowed to incubate for 3 days. At this time 10 µL of MTT (5 mg/mL) was added to each well and the 96-well plate was further incubated for 4 hours. Following the 4-hour incubation with MTT, 100 µL of SDS (10% w/v SDS, 0.01N HCl) was added to each well and incubated for an additional 4 hours. Absorbance values were then taken at 570 nm using a BioTek Synergy 2 Multimode Microplate Reader. Percent survival was calculated by dividing a treatment

absorbance by the control absorbance multiplied by 100. The log of concentration was plotted against percent survival in GraphPad Prism 6 to generate IC_{50} values for each compound. All values were generated through 3 biological replicates.

Pyruvate driven respitation assay using Seahorse XFe96 Analyzer

4T1 cells were seeded (20,000cells/well) onto Seahorse XFe96 well plates and incubated overnight in growth media at 37^{o}C and 5% CO_2. On the day of the assay, growth media was aspirated from the culture plates and replaced with mannitol/sucrose buffer (MAS; 70mM sucrose, 220mM mannitol, 10mM potassium phosphate monobasic, 5mM magnesium chloride, 2mM HEPES, and 1mM EGTA) and incubated at 37^{o}C in a non-CO_2 incubator. Port injections were prepared in MAS buffer and loaded at concentrations to allow for proper well concentration accounting for dilution factors (port injections A-D at 8X, 9X, 10X, and 11X concentrations). For these experiments test compound was injected in port A, followed by rPFO (1nM) in port B, followed by respective substrate cocktails (FCCP stimulated) in port C, and rotenone and antimycin A (0.5µM) in port D. Final substrate concentrations for specific tests were as follows: (5mM pyruvate, 0.5mM malate, 2mM dichloroacetate (DCA); 10mM glutamate, 0.5mM malate, 2mM DCA; 10mM succinate, 2µM rotenone; 20mM methyl pyruvate, 5mM pyruvate, 0.5mM malate, and 2mM DCA). ATP rate assays were performed according to the manufactures (Agilent) instructions.

3.C Spectral characterization of candidate compounds

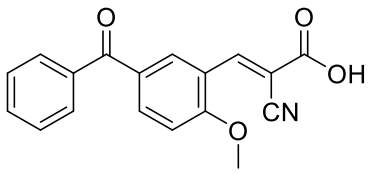

(*E*)-3-(5-benzoyl-2-methoxyphenyl)-2-cyanoacrylic acid

^{1}H NMR (400MHz, DMSO$_6$): δ 8.51 (s, 1H), 8.50 (d, 1H, 2.2Hz), 8.04 (dd, 1H, 2.16Hz, 6.6Hz), 7.77-7.76 (m, 2H), 7.69 (t, 1H, 7.4Hz), 7.58-7.54 (m, 2H), 7.39 (d, 1H, 8.9Hz), 4.02 (s, 3H)

^{13}C NMR (100MHz, DMSO$_6$): δ 194.09, 163.45, 162.12, 148.28, 137.34, 136.89, 133.01, 131.13, 129.94, 129.71, 129.11, 120.43, 116.13, 112.77, 105.95, 57.24

HRMS (ESI) m/z: calc'd for $C_{17}H_{16}O_5P$ $[M]^+$: 331.0730, found 331.0733

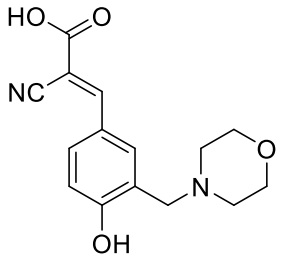

(*E*)-2-cyano-3-(4-hydroxy-3-(morpholinomethyl)phenyl)acrylic acid

^{1}H NMR (400MHz, DMSO$_6$): δ 8.13 (s, 1H), 7.99 (d, 1H, 2.2Hz), 7.88 (dd, 1H, 2.3Hz, 6.4Hz), 6.98 (d, 1H, 8.6Hz), 3.71 (s, 1H), 3.66 (t, 4H, 4.4Hz), 2.59 (s, 4H)

^{13}C NMR (100MHz, DMSO$_6$): δ 164.63, 161.85, 153.63, 133.80, 132.83, 123.20, 123.14, 117.69, 116.66, 100.53, 66.09, 57.27, 52.97

HRMS (ESI) m/z: calc'd for $C_{17}H_{16}O_5P$ $[M]^+$: 331.0730, found 331.0733

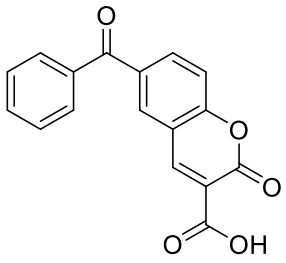

6-benzoyl-2-oxo-2H-chromene-3-carboxylic acid

Bibliography

(1) Tilg H, Moschen AR, Roden, M. NAFLD and diabetes mellitus. *Nat Rev Gastroenterol Hepatol* **2017**; 14: 32- 42.

(2) Lomonaco R, Bril F, Portillo-Sanchez P, Ortiz-Lopez C, Orsak B, Biernacki D, et al. Metabolic impact of nonalcoholic steatohepatitis in obese patients with type 2 diabetes. *Diabetes Care* **2016**; 39: 632- 638.

(3) Koliaki C, Szendroedi J, Kaul K, Jelenik T, Nowotny P, Jankowiak F, et al. Adaptation of hepatic mitochondrial function in humans with non-alcoholic fatty liver is lost in steatohepatitis. *Cell Metab* **2015**; 21: 739- 746.

(4) Gusdon A.M., Song K.X, Qu S. Nonalcoholic fatty liver disease: pathogenesis and therapeutics from a mitochondria-centric perspective. *Oxid Med Cell Longev* 2014; **2014**: 637027.

(5) Patterson RE, Kalavalapalli S, Williams CM, Nautiyal M, Mathew JT, Martinez J, et al. Lipotoxicity in steatohepatitis occurs despite an increase in tricarboxylic acid cycle activity. *Am J Physiol Endocrinol Metab* **2016**; 310: E484- 494.

(6) Satapati S, Kucejova B, Duarte JA, Fletcher JA, Reynolds L, Sunny NE, et al. Mitochondrial metabolism mediates oxidative stress and inflammation in fatty liver. *J Clin Invest* **2015**; 125: 4447- 4462.

(7) Friedman SL. Liver fibrosis in 2012: convergent pathways that cause hepatic fibrosis in NASH. *Nat Rev Gastroenterol Hepatol* **2013**; 10: 71– 72.

(8) Wallace MC, Friedman SL, Mann, DA. Emerging and disease-specific mechanisms of hepatic stellate cell activation. *Semin Liver Dis* **2015**; 35; 107- 118.

(9) Colca JS, et. al, Treating fatty liver disease by modulating mitochondrial pyruvate metabolism. Hepatology Communications **2017**; Vol. 1, No. 3

(10) McCommis KS, Finck BN. Mitochondrial pyruvate transport: a historical perspective and future research directions. Biochem J. **2015**;466:443–454.

(11) Satapati S, Sunny NE, Kucejova B, Fu X, He TT, et al. (**2012**) Elevated TCA cycle function in the pathology of diet-induced hepatic insulin resistance and fatty liver. J Lipid Res 53: 1080–1092.

(12) Sunny NE, Parks EJ, Browning JD, Burgess SC (**2011**) Excessive hepatic mitochondrial TCA cycle and gluconeogenesis in humans with nonalcoholic fatty liver disease. Cell Metab 14: 804–810.

(13) Patterson JN, Cousteils K, Lou JW, Manning Fox JE, MacDonald PE, Joseph JW. Mitochondrial metabolism of pyruvate is essential for regulating glucose-stimulated insulin secretion. J Biol Chem. **2014**;289:13335–13346.

(14) Colca, Jerry R et al. "Identification of a mitochondrial target of thiazolidinedione insulin sensitizers (mTOT)--relationship to newly identified mitochondrial pyruvate carrier proteins." *PloS one* vol. 8,5 e61551. 15 May. **2013**, doi:10.1371/journal.pone.0061551

(15) Bricker DK, Taylor EB, Schell JC, Orsak T, Boutron A, et al. (**2012**) A mitochondrial pyruvate carrier required for pyruvate uptake in yeast, *Drosophila*, and humans. Science 337: 96–100.

(16) Cusi K, Orsak B, Bril F, Lomonaco R, Hecht J, Ortiz-Lopez C, Tio F, et al. Long-Term Pioglitazone Treatment for Patients With Nonalcoholic Steatohepatitis and

Prediabetes or Type 2 Diabetes Mellitus: A Randomized, Controlled Trial. Ann Intern Med. **2016**

(17) Tontonoz P., Spiegelman B. M. Fat and beyond: the diverse biology of PPARgamma. *Annu. Rev. Biochem.* (**2008**);77:289–312. doi: 10.1146/annurev.biochem.77.061307.091829.

(18) Kahn BB, McGraw TE (**2010**) Rosiglitazone, PPARγ, and type 2 diabetes. N Engl J Med 363: 2667–2669.

(19) Chen Z, Vigueira PA, Chambers KT, Hall AM, Mitra MS, et al. (**2012**) Insulin resistance and metabolic derangements in obese mice are ameliorated by a novel peroxisome proliferator-activated receptor γ –sparing thiazolidinedione. J Biol Chem 287: 23537–23548.

(20) Musso G, Cassader M, Paschetta E, Gambino R. Thiazolidinediones and advanced liver fibrosis in nonalcoholic steatohepatitis: a meta-analysis. JAMA Intern Med **2017**; doi: 10.1001/jamainternmed.2016.9607.

(21) Neuschwander-Tetri BA, Brunt EM, Wehmeier KR, Oliver D, Bacon BR. Improved nonalcoholic steatohepatitis after 48 weeks of treatment with the PPAR-gamma ligand rosiglitazone. Hepatology **2003**; 38; 1008-1017.

(22) Caldwell SH, Patrie JT, Brunt EM, Redick JA, Davis CA, Park SH, et al. The effects of 48 weeks of rosiglitazone on hepatocyte mitochondria in human nonalcoholic steatohepatitis. Hepatology **2007**; 46:1101-1107.

(23) Ratziu V, Giral P, Jacqueminet S, Charlotte F, Hartemann-Heurtier A, Serfaty L, et al; Lido Study Group . Rosiglitazone for nonalcoholic steatohepatitis: one-year

results of the randomized placebo-controlled Fatty Liver Improvement with Rosiglitazone Therapy (FLIRT) Trial. Gastroenterology **2008**;135:100-110.

(24) Ratziu V, Charlotte F, Bernhardt C, Giral P, Halbron M, Lenaour G, et al; LIDO Study Group . Long-term efficacy of rosiglitazone in nonalcoholic steatohepatitis: results of the fatty liver improvement by rosiglitazone therapy (FLIRT 2) extension trial. Hepatology **2010**; 51:445-453.

(25) Sumida Y., Niki E., Naito Y., Yoshikawa T. Involvement of free radicals and oxidative stress in NAFLD/NASH. *Free Radical Research*. **2013**; 47(11):869–880. doi: 10.3109/10715762.2013.837577

(26) Kawano Y., Cohen D. E. Mechanisms of hepatic triglyceride accumulation in non-alcoholic fatty liver disease. *Journal of Gastroenterology*. **2013**; 48(4):434–441. doi: 10.1007/s00535-013-0758-5

(27) Browning J. D., Horton J. D. Molecular mediators of hepatic steatosis and liver injury. *The Journal of Clinical Investigation*. **2004**;114(2):147–152. doi: 10.1172/JCI200422422

(28) Brunt E. M., Kleiner D. E., Wilson L. A., Belt P., Neuschwander-Tetri B. A. Nonalcoholic fatty liver disease (NAFLD) activity score and the histopathologic diagnosis in NAFLD: distinct clinicopathologic meanings. *Hepatology*. **2011**;53(3):810–820. doi: 10.1002/hep.24127.

(29) Mari M, Caballero F, Colell A, Morales A, Caballeria J, Fernandez A, et al. Mitochondrial free cholesterol loading sensitizes to TNF- and Fas-mediated steatohepatitis. Cell Metab. **2006**; 4:185–98.

(30) Solsona-Vilarrasa, Estel et al. “Cholesterol enrichment in liver mitochondria impairs oxidative phosphorylation and disrupts the assembly of respiratory supercomplexes.” *Redox biology* vol. 24 (**2019**): 101214. doi:10.1016/j.redox.2019.101214

(31) Lanaspa MA, Sanchez-Lozada LG, Choi YJ, Cicerchi C, Kanbay M, Roncal-Jimenez CA, et al. Uric acid induces hepatic steatosis by generation of mitochondrial oxidative stress: potential role in fructose-dependent and -independent fatty liver. J Biol Chem. **2012**;287(48):40732–44.

(32) Lanaspa MA, Cicerchi C, Garcia G, Li N, Roncal-Jimenez CA, Rivard CJ, et al. Counteracting roles of AMP deaminase and AMP kinase in the development of fatty liver. PLoS One. **2012**; 7(11):e48801

(33) Jensen, Thomas et al. “Fructose and sugar: A major mediator of non-alcoholic fatty liver disease.” *Journal of hepatology* vol. 68,5 (**2018**): 1063-1075. doi:10.1016/j.jhep.2018.01.019

(34) Barrera F, George J. The role of diet and nutritional intervention for the management of patients with NAFLD. Clin Liver Dis. **2014**; 18:91–112

(35) Bouzianas DG, Bouziana SD, Hatzitolios AI. Potential treatment of human nonalcoholic fatty liver disease with long-chain omega-3 polyunsaturated fatty acids. Nutr Rev. **2013**; 71:753–771

(36) Masterton GS, Plevris JN, Hayes PC. Review article: omega-3 fatty acids - a promising novel therapy for non-alcoholic fatty liver disease. Aliment Pharmacol Ther. **2010**; 31:679–692

(37) Parker HM, Johnson NA, Burdon CA, Cohn JS, O'Connor HT, George J. Omega-3 supplementation and non-alcoholic fatty liver disease: a systematic review and meta-analysis. J Hepatol. **2012**; 56:944–951

(38) Corbet C, Linden C (2018) Killing two birds with one stone: Blocking the mitochondrial pyruvate carrier to inhibit lactate uptake by cancer cells and radiosensitize tumors, Molecular & Cellular Oncology, **2018** 5:4

(39) Gurrapu, S., Jonnalagadda, S. K., Alam, M. A., Ronayne, C. T., Nelson, G. L., Solano, L. N., Lueth, E. A., Drewes, L. R., & Mereddy, V. R. (**2016**). Coumarin carboxylic acids as monocarboxylate transporter 1 inhibitors: In vitro and in vivo studies as potential anticancer agents. *Bioorganic & medicinal chemistry letters*, *26*(14), 3282–3286.

(40) Lalonde, M. & Chan, T. Use of Organosilicon Reagents as Protective Groups in Organic Synthesis. *Synthesis (Stuttg).* 9, 817–854 (**1985**).

(41) Zhang, C.; Ondeyka, J. G.; Herath, K. B.; Guan, Z.; Collado, J.; Platas, G.; Pelaez, F.; Leavitt, P. S.; Gurnett, A.; Nare, (1) Zhang, C.; Ondeyka, J. G.; Herath, K. B.; Guan, Z.; Collado, J.; Platas, G.; Pelaez, F.; Leavitt, P. S.; Gurnett, A.; Nare, B.; Liberator, P.; Singh, S. B. Tenellones A and B from a Diaporthe Sp.: Two Highly Substituted Benzophenone Inhibitors of Parasite CGMP-Dependent Protein Kinase Activity. **2005**. https://doi.org/10.1021/np049591n.

(42) Paula, A.; Bernardi, M.; Ferraz, A. B. F.; Albring, D. V; Bordignon, S. A. L.; Schripsema, J.; Bridi, R.; Severo Dutra-Filho, C.; Henriques, A. T.; Lino Von Poser, G. Benzophenones from Hypericum Carinatum. **2005**.

https://doi.org/10.1021/np040149e.

(43) Yoganathan, K.; Cao, S.; Crasta, S. C.; Aitipamula, S.; Whitton, S. R.; Ng, S.; Buss, A. D.; Butler, M. S. Microsphaerins A-D, Four Novel Benzophenone Dimers with Activity against MRSA from the Fungus Microsphaeropsis Sp. **2008**. https://doi.org/10.1016/j.tet.2008.08.038.

(44) Wu, X. De; Cheng, J. T.; He, J.; Zhang, X. J.; Dong, L. Bin; Gong, X.; Song, L. D.; Zheng, Y. T.; Peng, L. Y.; Zhao, Q. S. Benzophenone Glycosides and Epicatechin Derivatives from Malania Oleifera. *Fitoterapia* **2012**, *83* (6), 1068–1071. https://doi.org/10.1016/j.fitote.2012.05.006.

(45) F. Bosca, M. A. Miranda, G. Carganico and D. Mauleon, Photochem. Photobiol., **1994**, 60, 96–101.

(46) F. Bosca and M. A. Miranda, J. Photochem. Photobiol., B, **1998**, 43, 1–26.

(47) M. C. Cuquerella, V. Lhiaubet-Vallet, J. Cadet and M. A. Miranda, Acc. Chem. Res., **2012**, 45, 1558–1570.

(48) J. Leegwater-Kim and C. Waters, Expert Rev. Neurother., **2007**, 7, 1649–1657.

(49) R. S. Rosenson, Expert Rev. Cardiovasc. Ther., **2008,** 6, 1319–1330.

(50) M. A. Forbes, Jr., M. Brannen and W. C. King, South. Med. J., **1966**, 59, 321–324.

(51) A. R. Heurung, S. I. Raju and E. M. Warshaw, Dermatitis, **2014**, 25, 3–10.

(52) J. R. Gibson, Cutis, **1993**, 51, 406.

(53) S. A. Khanum, S. Shashikanth and A. V. Deepak, Bioorg. Chem., **2004**, 32, 211–222.

(54) C. Liu, J. Jin, L. Chen, J. Zhou, X. Chen, D. Fu, H. Song and B. Xu, Bioorg. Med. Chem., **2012**, 20, 2992–2999.

(55) K. Vinaya, C. V. Kavitha, D. S. Prasanna, S. Chandrappa, S. R. Ranganatha, S. C. Raghavan and K. S. Rangappa, Chem. Biol. Drug Des., **2012**, 79, 360–367.

(56) F. Belluti, L. Piazzi, A. Bisi, S. Gobbi, M. Bartolini, A. Cavalli, P. Valenti and A. Rampa, Eur. J. Med. Chem., **2009**, 44, 1341–1348.

(57) Jonnalagadda S., Jonnalagadda S. K., Ronayne C. T., Nelson G. L., Solano L. N., Rumbley J., Holy J., Mereddy V. R., Drewes L. R. Novel N,N-dialkyl cyanocinnamic acids as monocarboxylate transporter 1 and 4 inhibitors. *Oncotarget.* ***2019****; 10*: 2355-2368.

(58) Surana, K., Chaudhary, B., Diwaker, M., & Sharma, S. (**2018**). Benzophenone: a ubiquitous scaffold in medicinal chemistry. *MedChemComm*, *9*(11), 1803-1817.

(59) Arend, M., Westermann, B., & Risch, N. (**1998**). Modern variants of the Mannich reaction. *Angewandte Chemie International Edition*, *37*(8), 1044-1070.

(60) Sonveaux, P., Végran, F., Schroeder, T., Wergin, M. C., Verrax, J., Rabbani, Z. N., ... & Kelley, M. J. (**2008**). Targeting lactate-fueled respiration selectively kills hypoxic tumor cells in mice. *The Journal of clinical investigation*, *118*(12), 3930-3942.

(61) Kourounakis, A. P., Xanthopoulos, D., & Tzara, A. (**2020**). Morpholine as a privileged structure: A review on the medicinal chemistry and pharmacological activity of morpholine containing bioactive molecules. *Medicinal Research Reviews*, *40*(2), 709-752.

(62) Halestrap, A. P. (**1975**). The mitochondrial pyruvate carrier. Kinetics and specificity for substrates and inhibitors. *Biochemical Journal*, *148*(1), 85-96.

(63) Corbet, C., Bastien, E., Draoui, N., Doix, B., Mignion, L., Jordan, B. F.,Becker, H. M. **2018**. Interruption of lactate uptake by inhibiting mitochondrial pyruvate transport unravels direct antitumor and radiosensitizing effects. *Nature communications*, *9*(1), 1-1

(64) Darwish KM, Salama I, Mostafa S, Gomaa MS, Helal MA. Design, synthesis, and biological evaluation of novel thiazolidinediones as PPARγ/FFAR1 dual agonists. *Eur J Med Chem***. 2016**;109:157-172. doi:10.1016/j.ejmech.2015.12.049

Appendix

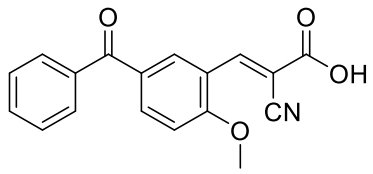
O
O
OH
CN
O

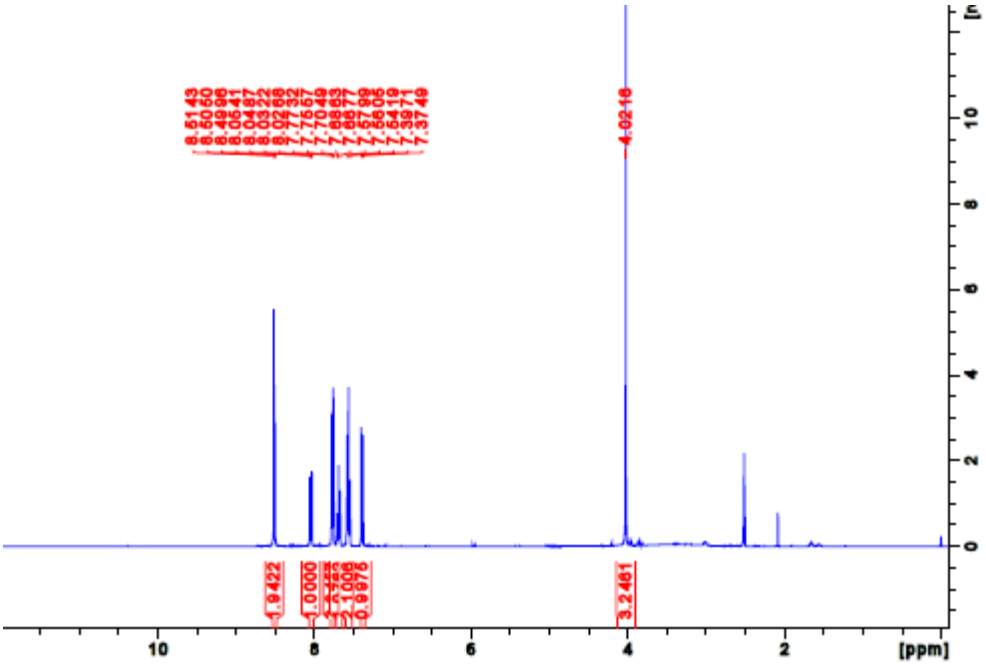
8.5143
8.5050
8.4996
8.0541
8.0487
8.0322
8.0268
7.7732
7.7667
7.7049
7.6963
7.6877
7.5799
7.5605
7.5419
7.3971
7.3749
4.0216
1.9422
1.0000
3.2461
10
8
6
4
2
[ppm]
0
2
4
6
8
10

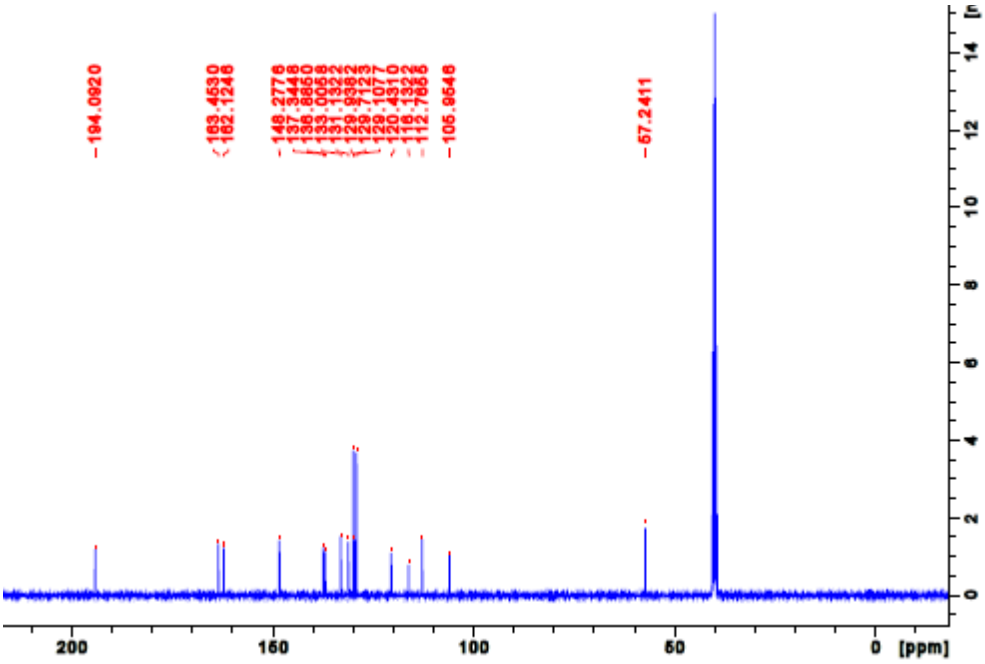
194.0920
163.4530
162.1246
148.2776
137.3448
136.8860
133.0058
131.1322
129.9382
129.7123
129.1077
120.4310
118.1322
112.7865
105.9646
67.2411
200
150
100
50
0
[ppm]

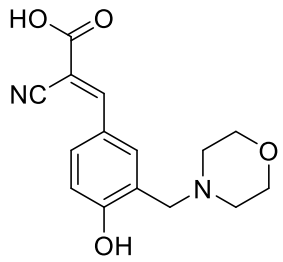
HO
O
NC
O
N
OH

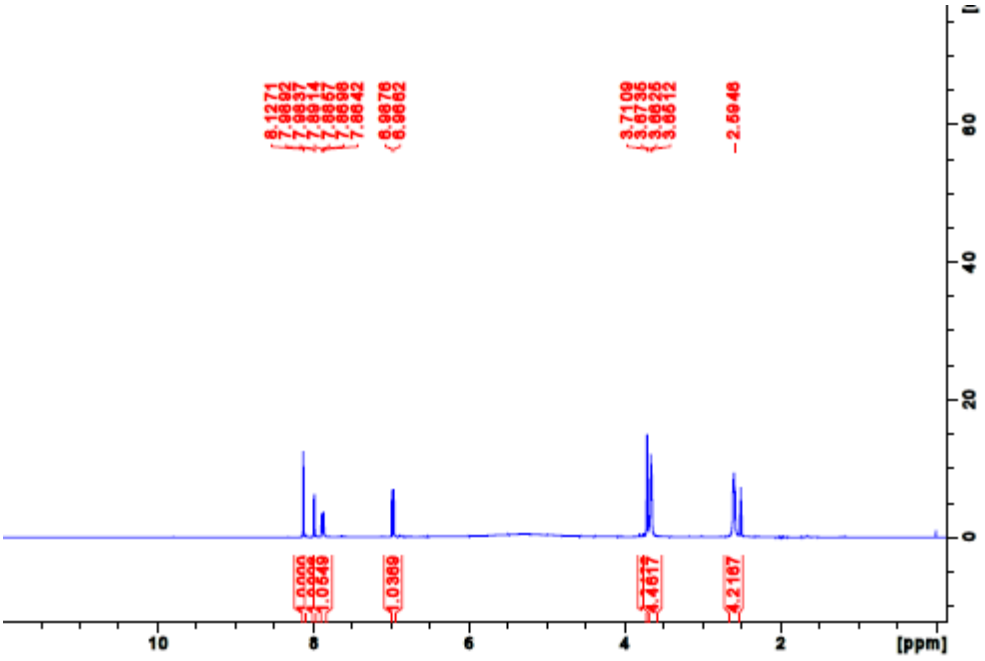
8.1271
7.9892
7.9837
7.8914
7.8867
7.8698
7.8642
6.9876
6.9662
3.7109
3.6736
3.6625
3.6512
2.5946
1.0000
1.0004
1.0649
1.0369
4.4617
4.2167
10
8
6
4
2
[ppm]
0
20
40
60

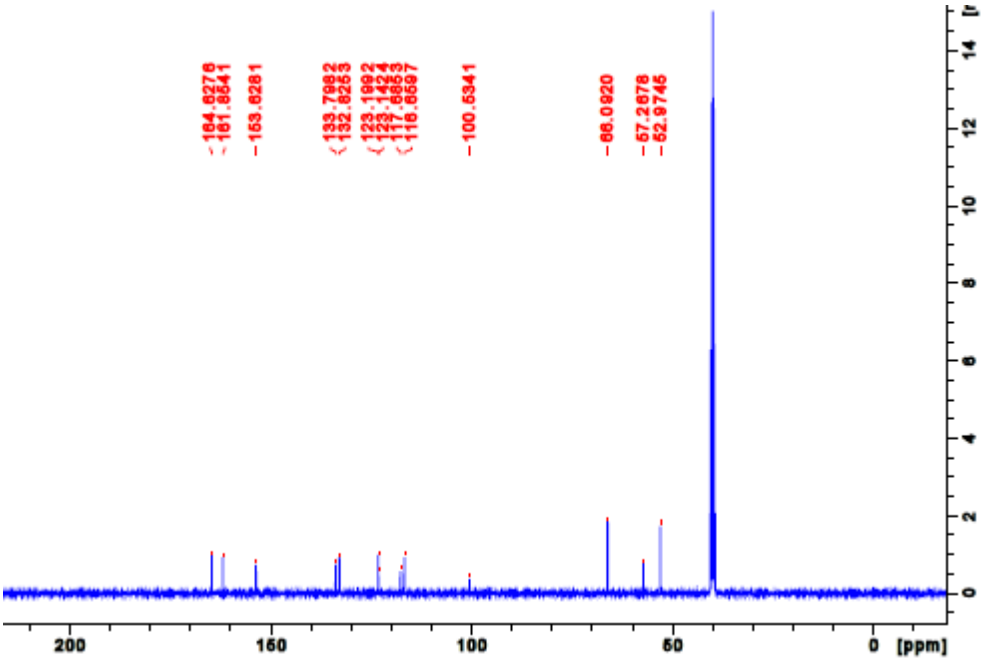
164.6276
161.8641
163.6281
133.7882
132.8253
123.1992
123.1424
117.6853
116.6587
100.5341
66.0920
67.2678
62.9745
200
150
100
50
0
[ppm]